

An Eddy–Zonal Flow Feedback Model for Propagating Annular Modes

SANDRO W. LUBIS^a AND PEDRAM HASSANZADEH^a

^a*Rice University, Houston, Texas*

(Manuscript received 16 July 2020, in final form 12 October 2020)

ABSTRACT: The variability of the zonal-mean large-scale extratropical circulation is often studied using individual modes obtained from empirical orthogonal function (EOF) analyses. The prevailing reduced-order model of the leading EOF (EOF1) of zonal-mean zonal wind, called the annular mode, consists of an eddy–mean flow interaction mechanism that results in a positive feedback of EOF1 onto itself. However, a few studies have pointed out that under some circumstances in observations and GCMs, strong couplings exist between EOF1 and EOF2 at some lag times, resulting in decaying-oscillatory, or propagating, annular modes. Here, we introduce a reduced-order model for coupled EOF1 and EOF2 that accounts for potential cross-EOF eddy–zonal flow feedbacks. Using the analytical solution of this model, we derive conditions for the existence of the propagating regime based on the feedback strengths. Using this model, and idealized GCMs and stochastic prototypes, we show that cross-EOF feedbacks play an important role in controlling the persistence of the annular modes by setting the frequency of the oscillation. We find that stronger cross-EOF feedbacks lead to less persistent annular modes. Applying the coupled-EOF model to the Southern Hemisphere reanalysis data shows the existence of strong cross-EOF feedbacks. The results highlight the importance of considering the coupling of EOFs and cross-EOF feedbacks to fully understand the natural and forced variability of the zonal-mean large-scale circulation.

KEYWORDS: Annular mode; Atmospheric circulation; Dynamics; Eddies; Climate variability

1. Introduction

At the intraseasonal to interannual time scales, the variability of the large-scale atmospheric circulation in the mid-latitudes of both hemispheres is dominated by the “annular modes,” which are usually defined based on empirical orthogonal function (EOF) analysis of zonal-mean meteorological fields (e.g., Kidson 1988; Thompson and Wallace 1998, 2000; Lorenz and Hartmann 2001, hereafter LH01, 2003; Thompson and Woodworth 2014; Thompson and Li 2015). The barotropic annular modes are often derived as the first (i.e., leading) EOF (EOF1) of zonal-mean zonal wind, which exhibits a dipolar meridional structure and describes a north–south meandering of the eddy-driven jet. Note that in this paper, the focus is on the barotropic annular modes, hereafter simply called annular modes [see Thompson and Woodworth (2014), Thompson and Barnes (2014), and Thompson and Li (2015) for discussions about the “baroclinic annular modes”]. The second EOF of zonal-mean zonal wind (EOF2) has a tripolar meridional structure centered on the jet, describing a strengthening and narrowing of the eddy-driven jet (i.e., jet pulsation). By construction, EOF1 and EOF2 (and any two EOFs) are orthogonal and their associated time series [i.e., principal components (PCs)], sometimes called zonal index, are independent at zero time lag.

The persistence of the annular mode (EOF1) and its underlying dynamics have been the subject of extensive research and debate in the past three decades (e.g., Robinson 1991; Branstator 1995; Feldstein and Lee 1998; Robinson 2000; Limpasuvan and Hartmann 1999; LH01; Lorenz and Hartmann 2003; Gerber and Vallis 2007; Gerber et al. 2008b; Chen and Plumb 2009; Simpson et al. 2013; Zurita-Gotor 2014; Nie et al. 2014;

Byrne et al. 2016; Ma et al. 2017; Hassanzadeh and Kuang 2019). Many of the aforementioned studies have pointed to a positive eddy–zonal flow feedback mechanism as the source of the persistence: The zonal wind, meridional wind, and temperature anomalies associated with the annular mode (EOF1) modify the generation and/or propagation of the synoptic eddies at the quasi-steady limit (on long time scales) in such a way that the resulting eddy fluxes reinforce the annular mode (see Hassanzadeh and Kuang 2019, and the discussion and references therein). Most notably, LH01 developed a linear eddy–zonal flow feedback model for the annular modes by regressing the anomalous eddy momentum flux divergence onto the zonal index of EOF1 [$z_1(t)$] and interpreting positive correlations between $z_1(t)$ and regressed momentum flux divergence [$m_1(t)$] at long lags (greater than 7 days) as evidence for positive eddy–zonal flow feedbacks, i.e., positive feedbacks of EOF1 onto itself.¹ LH01 developed a similar model separately for EOF2 and found weak eddy–zonal flow feedbacks for EOF2, consistent with the longer persistence of EOF1 compared to EOF2. Such single-EOF eddy–zonal flow feedback models have been used in most of the subsequent studies of the annular modes (e.g., Lorenz and Hartmann 2003; Simpson et al. 2013; Lorenz 2014; Robert et al. 2017; Ma et al. 2017; Boljka et al. 2018; Hassanzadeh and Kuang 2019; Lindgren et al. 2020).

While EOF1 and EOF2 are independent at zero lag, a few previous studies have pointed out that these two EOFs can be

¹ It is worth mentioning that recently, some studies have suggested external (to the troposphere) influences, e.g., from nonstationary interannual variability and stratospheric polar vortex, rather than internal (to the troposphere) eddy–zonal flow feedbacks, as the cause of these positive correlations between z_1 and m_1 (Byrne et al. 2016; Saggiaro and Shepherd 2019).

Corresponding author: Sandro Wellyanto Lubis, slubis@rice.edu

DOI: 10.1175/JAS-D-20-0214.1

© 2020 American Meteorological Society. For information regarding reuse of this content and general copyright information, consult the AMS Copyright Policy (www.ametsoc.org/PUBSReuseLicenses).

correlated at long lags (i.e., greater than 7 days), and that in fact the combination of these two leading EOFs represents coherent meridional propagations of the zonal-mean flow anomalies. Such propagating regimes have been observed in both hemispheres in reanalysis data (e.g., [Feldstein 1998](#); [Feldstein and Lee 1998](#); [Sheshadri and Plumb 2017](#)). Anomalous poleward propagation of zonal wind typically emerges in low latitudes and mainly migrate poleward over a few months, although non-propagating regimes can also appear in some instances [see Fig. 1 of [Sheshadri and Plumb \(2017\)](#) and Fig. 6 in this paper]. Similar behaviors have also been reported by in general circulation models (GCMs) (e.g., [James and Dodd 1996](#); [Son and Lee 2006](#); [Son et al. 2008](#); [Sparrow et al. 2009](#); [Sheshadri and Plumb 2017](#)). [Son and Lee \(2006\)](#) found that the leading mode of variability in an idealized dry GCM can be either the propagating or nonpropagating regime depending on the details of thermal forcing imposed in the model. They also found that unlike the nonpropagating regimes, the z_1 and z_2 of the propagating regimes are strongly correlated at long lags, peaking at around 48 days (see their Fig. 3 and Fig. 4b of the present paper). The statistically significant cross correlation between z_1 and z_2 at long lags indicates that positive PC1 leads to positive PC2, and positive PC2 leads to negative PC1. Given the relative structure of the EOFs, this cross correlation describes the poleward propagation of zonal wind anomalies. Furthermore, [Son and Lee \(2006\)](#) reported that nonpropagating regimes are often characterized by a single time-mean jet with a dominant EOF1 (in terms of the explained variance) while the propagating regimes are characterized by a double time-mean jet in the midlatitudes with the variance associated with EOF2 being at least half of the variance of EOF1. Such differences in the structure and position of the jet can affect the propagation of Rossby waves by changing the critical latitude dynamics (e.g., [Lee et al. 2007](#); [Ronalds et al. 2018](#)), resulting in different eddy-mean flow interaction characteristics and hence, different characteristics of the annular modes. Furthermore, [Son et al. \(2008\)](#) found the e -folding decorrelation time scale of z_1 in the propagating regime to be much shorter than that of the nonpropagating regime. The long e -folding decorrelation time scales for the annular modes in the nonpropagating regime were attributed to an unrealistically strong positive EOF1-onto-EOF1 feedback, while the reason behind the reduction in the persistence of the annular modes in the propagating regime remained unclear.

More recently, [Sheshadri and Plumb \(2017\)](#) presented further evidence for the existence of propagating and nonpropagating regimes and strong lagged correlations between z_1 and z_2 in reanalysis data of the Southern Hemisphere (SH) and in idealized GCMs. Moreover, they elegantly showed, using a principal oscillation pattern (POP) analysis ([Hasselmann 1988](#); [Penland 1989](#)), that EOF1 and EOF2 are in fact manifestations of a single, decaying-oscillatory coupled mode of the dynamical system. Specifically, they found that EOF1 and EOF2 are, respectively, the real and imaginary parts of a single POP mode, which describes the dominant aspects of the spatiotemporal evolution of zonal wind anomalies. [Sheshadri and Plumb \(2017\)](#) also showed that in the propagating regime, the autocorrelation functions of z_1 and z_2 decay nonexponentially.

Given the above discussion, a single-EOF model is not enough to describe a propagating regime because the EOF1 and EOF2 in this regime are strongly correlated at long lags and the autocorrelation functions of the associated PCs do not decay exponentially (but rather show some oscillatory behaviors as well). From the perspective of eddy-zonal flow feedbacks, one may wonder whether there are cross-EOF feedbacks in addition to the previously studied EOF1 (EOF2) eddy-zonal flow feedback onto EOF1 (EOF2) in the propagating regime. In cross-EOF feedbacks, EOF1 (EOF2) changes the eddy forcing of EOF2 (EOF1) in the quasi-steady limit. Therefore, there is a need to extend the single-EOF model of [LH01](#) and build a model that includes, at a minimum, both leading EOFs and accounts for their cross feedbacks. The objective of the current study is to develop such a model and to use it to estimate effects of the cross-EOF feedbacks on the variability of propagating annular modes.

The paper is structured as follows: [Section 2](#) compares the characteristics of z_1 , z_2 , m_1 , and m_2 for the nonpropagating and propagating annular modes in reanalysis and idealized GCMs. In [section 3](#), we develop a linear eddy-zonal flow feedback model that accounts for cross-EOF feedbacks, validate the model using synthetic data from a stochastic prototype, discuss the key properties of the analytical solution of this model, and apply this model to data from reanalysis and an idealized GCM. The paper ends with concluding remarks in [section 4](#).

2. Propagating annular modes in an idealized GCM and reanalysis

In this section, we will examine the basic characteristics and statistics of propagating annular modes in an idealized GCM (the dry dynamical core) and reanalysis. We focus on the southern annular mode, which makes it easier to compare the results of the reanalysis and the idealized GCM simulations. We will start with the idealized GCM to demonstrate the characteristics of the propagating and nonpropagating annular modes.

a. An idealized GCM: The dry dynamical core

We use the Geophysical Fluid Dynamics Laboratory (GFDL) dry dynamical core GCM. The GCM is run with a flat, uniform lower boundary with T63 spectral resolution and 40 evenly spaced sigma levels in the vertical for 50 000-day integrations after spinup. The physics of the model is based on [Held and Suarez \(1994\)](#), an idealized configuration for generating a realistic global circulation with minimal parameterization ([Held 2005](#); [Jeevanjee et al. 2017](#)). All diabatic processes are represented by Newtonian relaxation of the temperature field toward a prescribed equilibrium profile, and Rayleigh friction is included in the lower atmosphere to mimic the interactions with the boundary layer.

The nonpropagating and propagating regimes are produced in two slightly different setups of this model. For the setup with the nonpropagating regime, we use the standard configuration of [Held and Suarez \(1994\)](#), which employs an analytical profile approximating a troposphere in unstable radiative-convective equilibrium and an isothermal stratosphere for Newtonian relaxation. For the setup with the propagating regime, we follow an

approach similar to the one used by Sheshadri and Plumb (2017). In this setup, for the equilibrium temperature profile in the troposphere and stratosphere, we use the perpetual-solstice version of the equilibrium-temperature specifications used in Lubis et al. (2018a), calculated from a Rapid Radiative Transfer Model (RRTM), with winter conditions in the SH. As will be seen later, these choices result in a large-scale circulation with overall reasonable annular mode time scales in the SH.

In Fig. 1, we show, following Son and Lee (2006), the one-point lag-correlation maps for the zonal-mean zonal wind anomalies integrated across the depth of the troposphere (1000–100 hPa) $\langle \bar{u} \rangle$ reconstructed from projections onto the two leading EOFs of $\langle \bar{u} \rangle$ for the two setups (hereafter, angle brackets and overbars denote the vertical and zonal averages, respectively). The anomalies are defined as the deviations from the time mean. The nonpropagating and propagating regimes are clearly seen in Figs. 1a and 1b, respectively. In the latter, the propagating anomalies emerge in low latitudes and propagate generally poleward over the course of 3–4 months, consistent with Sheshadri and Plumb (2017). In contrast, the nonpropagating regime is characterized by persistent zonal flow anomalies in the midlatitudes (Fig. 1a).

To understand the relationship between zonal-mean zonal wind and eddy forcing in the nonpropagating and propagating annular modes, the vertically averaged zonal-mean zonal wind anomalies ($\langle \bar{u} \rangle$) and vertically averaged zonal-mean eddy momentum flux convergence anomalies ($\langle \bar{F} \rangle$) are projected onto the leading EOFs of $\langle \bar{u} \rangle$ following LH01. The time series of zonal index (z) and eddy forcing (m) associated with EOF1 and EOF2 are formulated as

$$z_{1,2}(t) = \frac{\langle \bar{\mathbf{u}} \rangle(t) \mathbf{W} \mathbf{e}_{1,2}}{\sqrt{\mathbf{e}_{1,2}^T \mathbf{W} \mathbf{e}_{1,2}}}, \quad (1)$$

$$m_{1,2}(t) = \frac{\langle \bar{\mathbf{F}} \rangle(t) \mathbf{W} \mathbf{e}_{1,2}}{\sqrt{\mathbf{e}_{1,2}^T \mathbf{W} \mathbf{e}_{1,2}}}, \quad (2)$$

where $z_{1,2}$ ($m_{1,2}$) denotes the component of the field $\langle \bar{\mathbf{u}} \rangle$ ($\langle \bar{\mathbf{F}} \rangle$) that projects onto the latitudinal structure of the two leading EOFs. The superscript T means transpose. Other terms are as follows: $\langle \bar{\mathbf{u}} \rangle(t)$ and $\langle \bar{\mathbf{F}} \rangle(t)$ are $\langle \bar{\mathbf{u}} \rangle(\phi, t)$ and $\langle \bar{\mathbf{F}} \rangle(\phi, t)$ with their latitude dimension vectorized, \mathbf{W} is a diagonal matrix whose elements are the $\cos(\phi)$ weightings used when defining the EOF structure \mathbf{e} , and ϕ is latitude (Simpson et al. 2013; Ma et al. 2017). Here, the vertically averaged zonal-mean eddy momentum flux convergence ($\langle \bar{F} \rangle$) is calculated in the spherical coordinate as

$$\langle \bar{F} \rangle(\phi, t) = -\frac{1}{\cos^2 \phi} \frac{\partial(\langle \bar{u}'v' \cos^2 \phi \rangle)}{a \partial \phi}, \quad (3)$$

where u' and v' are deviations of zonal wind and meridional wind from their respective zonal means, and a is Earth's radius.

Figure 2 shows lagged-correlation analysis between z and m in the GCM setup with nonpropagating regime. The autocorrelation of z_1 , as discussed in past studies (e.g., Chen and Plumb 2009; Ma et al. 2017), has a noticeable shoulder at around 5-day lags and shows an unrealistically persistent annular mode, well separated from the faster decaying z_2 , which is consistent with

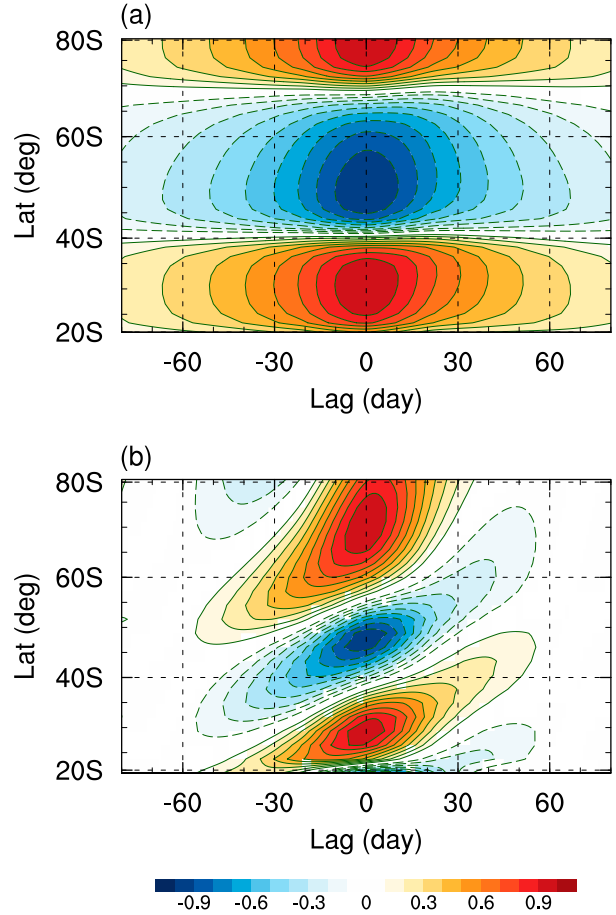


FIG. 1. One-point lag-correlation maps of the zonal-mean zonal wind anomalies integrated across the depth of the troposphere (1000–100 hPa) $\langle \bar{u} \rangle$, reconstructed from projections onto the two leading EOFs of $\langle \bar{u} \rangle$ for the (a) nonpropagating regime and (b) propagating regime in two setups of an idealized GCM. The base latitude is at 30°S. The contour line interval is 0.1. Solid contour lines are positive, dashed contours lines are negative, and the zero contour line is omitted. Color shading denotes values significant at the 95% level according to the t test.

the considerable difference in the contribution of the two EOFs to the total zonal wind variance (60.2% vs 19.2%). The e -folding decorrelation time scales of z_1 and z_2 are 64.5 and 4.8 days, respectively. The strong, positive cross correlations of $m_1 z_1$ and insignificant cross correlations of $m_2 z_2$ at large positive lags suggest the existence of a positive eddy–zonal flow feedback for EOF1 (from EOF1) but not for EOF2 (from EOF2) (see Son et al. 2008; Ma et al. 2017). Figure 2b shows that the $z_1 z_2$ cross correlations are weak at positive and negative lags, which are consistent with the one-point lag-correlation map of Figs. 1a and 3 (shown later), and are indicative of a nonpropagating regime, as reported previously for a similar setup (Son and Lee 2006; Son et al. 2008). The $m_1 z_2$ and $m_2 z_1$ cross correlations are small and often insignificant, suggesting the absence of the cross-EOF feedbacks in the nonpropagating regime (Figs. 2e,f). All together, the above

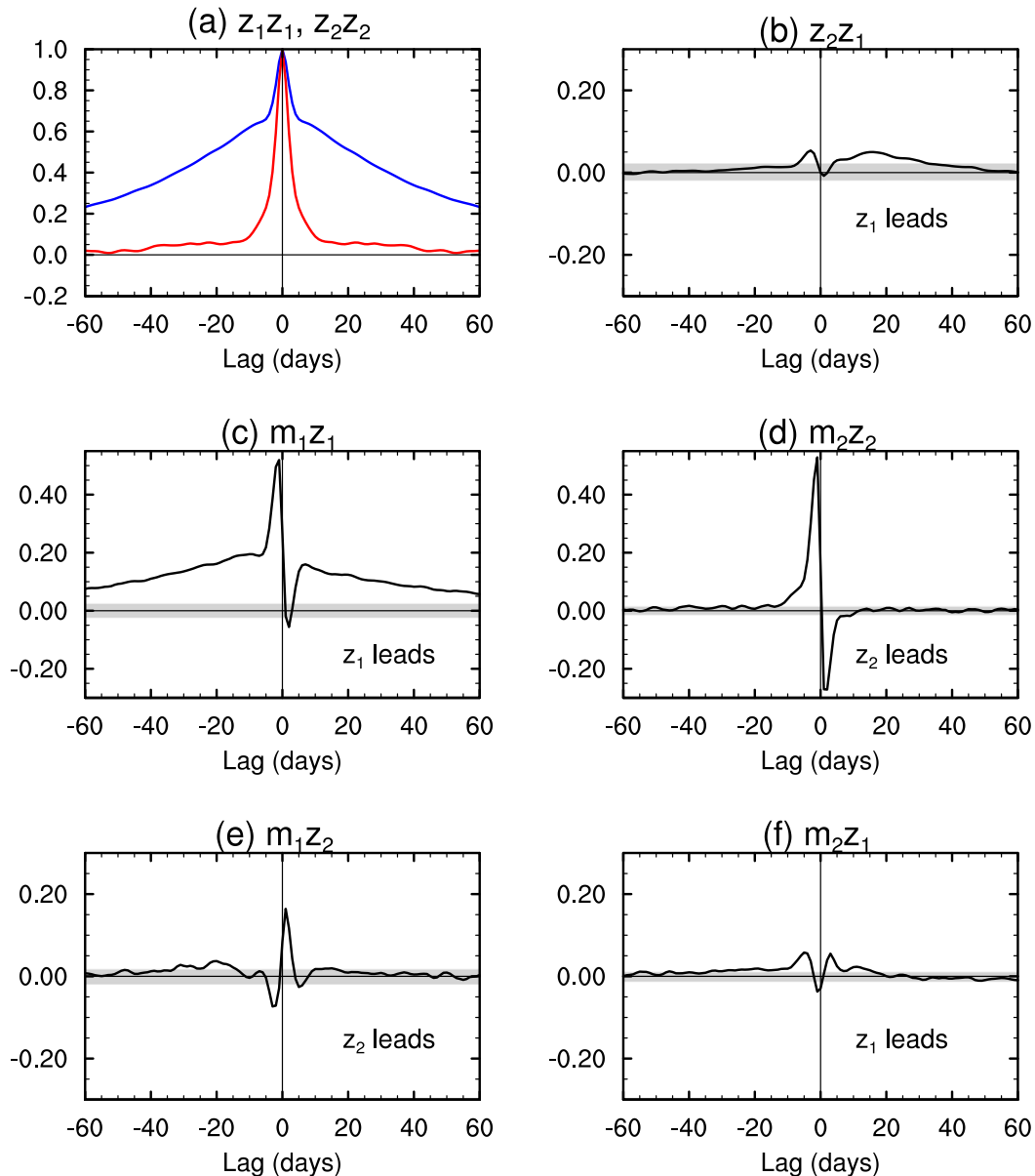


FIG. 2. Lagged-correlation analysis of the GCM setup with nonpropagating regime. (a) Autocorrelation of z_1 (blue) and z_2 (red), (b) cross-correlation $z_1 z_2$, (c) cross-correlation $m_1 z_1$, (d) cross-correlation $m_2 z_2$, (e) cross-correlation $m_1 z_2$, and (f) cross-correlation $m_2 z_1$. The two leading EOFs contribute 60.2% and 19.2%, respectively, to the total variance. The e -folding decorrelation time scales of z_1 and z_2 are 64.5 and 4.8 days, respectively. Gray shading represents 5% significance level according to the test of Bartlett ([appendix](#)).

analysis shows that for the nonpropagating regime, single-EOF reduced-order models such as LH01 are sufficient.

The weak cross correlations between z_1 and z_2 in the GCM with the nonpropagating regime (Fig. 2b) can be also seen by regressing the zonal-mean zonal wind anomalies on the zonal index at 0- and 20-day time lags. Figures 3a and 3b show the wind anomalies regressed on z_1 and z_2 at lag 0, yielding approximately the EOF1 and EOF2 patterns, respectively. Twenty days after z_1 leads zonal wind anomalies, the anomalies do not drift poleward or decay, but rather persist (Fig. 3d). In contrast, 20 days after z_2

leads zonal wind anomalies, the anomalies decay and disappear (Fig. 3c). These observations are consistent with the long and short persistence of z_1 and z_2 , respectively, consistent with the weak cross correlations of z_1 and z_2 at positive or negative lags, and as it becomes clear below, consistent with the nonpropagating nature of this setup.

Figure 4 shows lagged-correlation analysis between z and m in the GCM setup with propagating regime. The autocorrelation of z_1 , its persistence compared to that of z_2 , and the explained variance by the two EOFs (40.4% versus 32.5%) are much more

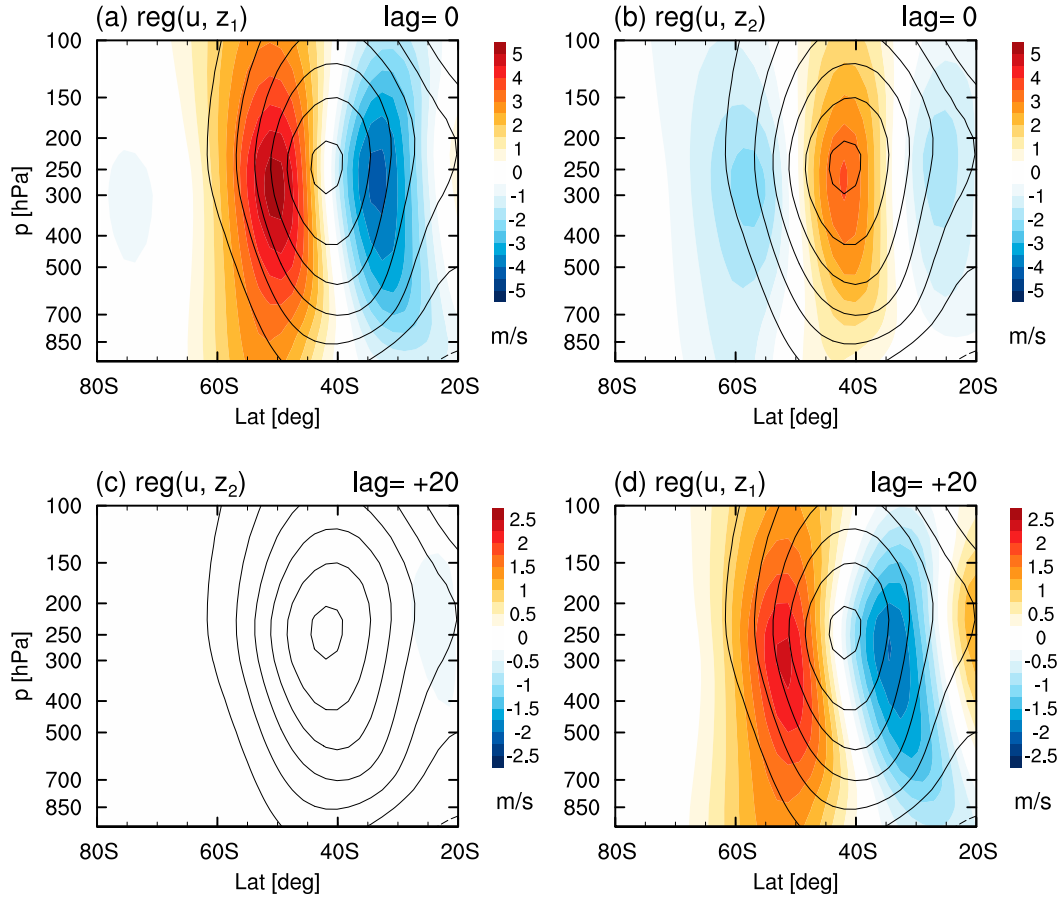


FIG. 3. Anomalous zonal-mean zonal wind (\bar{u}) regressed onto z_1 and z_2 in the GCM setup with nonpropagating regime: (a), (b) simultaneous, (c) z_2 leads by 20 days, and (d) z_1 leads by 20 days. The contours are the climatological zonal-mean zonal wind with interval of 5 m s^{-1} .

similar to what is observed in the SH (shown later in Fig. 7). The e -folding decorrelation time scales of z_1 and z_2 are 14.1 and 9.2 days, respectively. Figure 4b shows that z_1 and z_2 are strongly correlated at long lags peaking at around ± 20 days. This behavior along with the one-point lag-correlation map of Fig. 1b and regression map of wind anomalies (Fig. 5, shown later) suggests the existence of a propagating regime, as noted by few previous studies (e.g., Son and Lee 2006; Sheshadri and Plumb 2017). It should be noted that Son and Lee (2006) have proposed a rule of thumb based on the ratio of the explained variance of EOF2 to EOF1: a nonpropagating (propagating) regimes exists if the ratio is smaller (larger) than 0.5. The regimes of our two setups are consistent with this rule of thumb as the ratios are ~ 0.3 and ~ 0.8 in our nonpropagating and propagating regimes.

Furthermore, Fig. 4c shows that the $m_1 z_1$ cross correlations are positive at long positive lags (5–20 days) and then negative but small. Figure 4d indicates weak positive cross correlations at lags 5–10 days and weak negative cross correlations at the timescale of longer than 20 days between z_2 and m_2 (Fig. 4c). Overall, the shape of the $m_1 z_1$ and $m_2 z_2$ cross-correlation functions are similar between the nonpropagating and

propagating regimes, although the $m_1 z_1$ cross correlations are larger and more persistent in the nonpropagating regime. In contrast, the $m_1 z_2$ and $m_2 z_1$ cross correlations are substantially different between the two regimes (Figs. 4e,f). There are statistically significant and large positive $m_1 z_2$ cross correlations at large positive lags (> 5 days) and statistically significant and large negative $m_2 z_1$ cross correlations at positive lags up to 30 days. Note that as emphasized in the figures, positive lags here mean that z_1 (z_2) is leading m_2 (m_1). Therefore, these cross correlations, as discussed later, indicate the existence of cross-EOF feedbacks in the propagating regime.

Figure 5 shows anomalous zonal-mean zonal wind regressed on z_1 and z_2 at 0- and 20-day time lags in the GCM setup with propagating regime. Figures 5a and 5b show the wind anomalies regressed on z_1 and z_2 at lag 0, again yielding approximately the EOF1 and EOF2 patterns, respectively. As shown in Fig. 5c, 20 days after z_2 leads zonal wind anomalies, the anomalies have drifted poleward and project strongly onto the structure of wind anomalies associated with EOF1 (Figs. 5a,c; pattern correlation = 0.93). This is consistent with positive correlation of $z_1 z_2$ at lag +20 days when z_1 leads z_2 (Fig. 4b). Likewise, 20 days after z_1 leads zonal wind anomalies, the

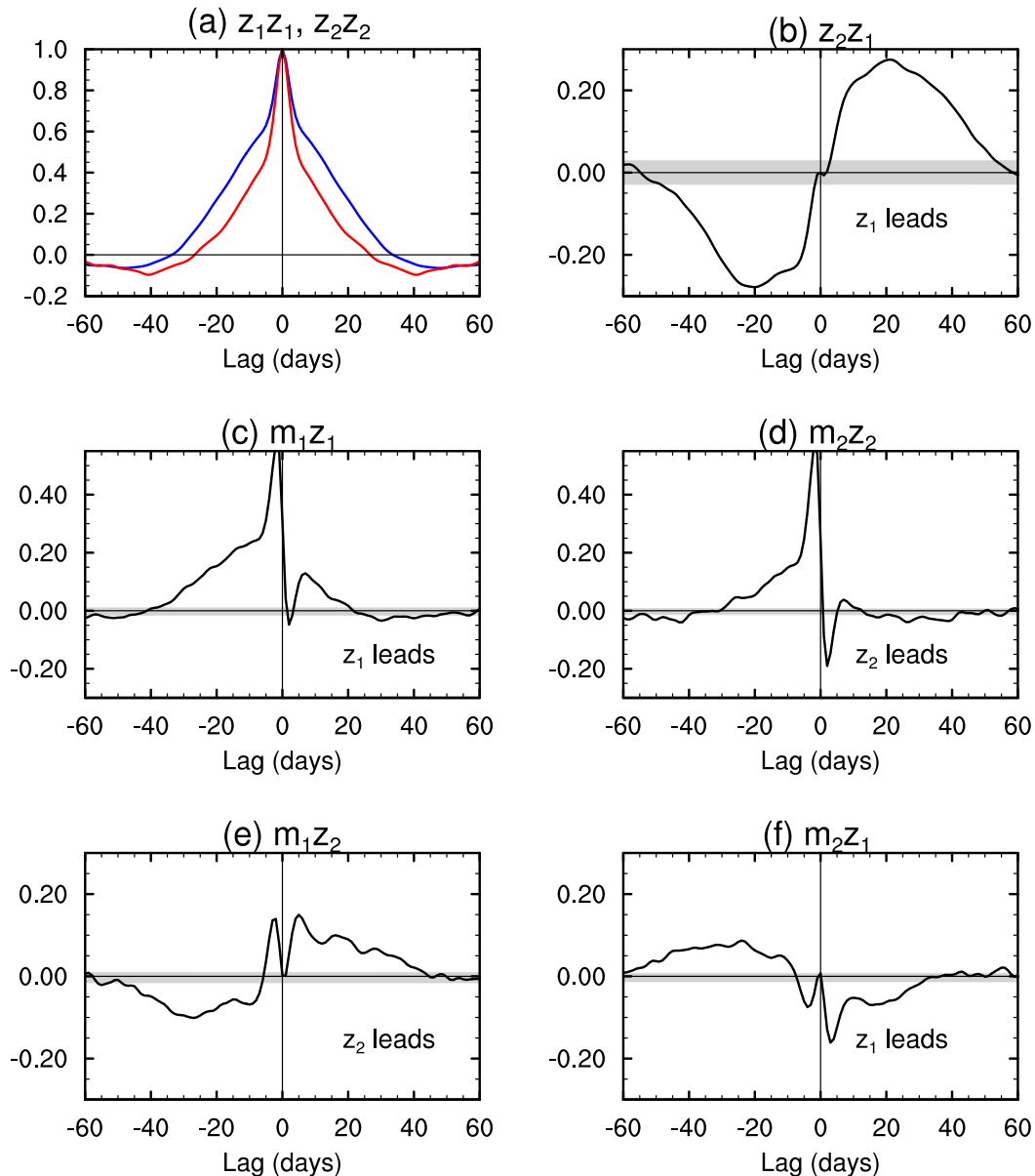


FIG. 4. Lagged-correlation analysis of the GCM setup with propagating regime. (a) Autocorrelation of z_1 (blue) and z_2 (red), (b) cross-correlation z_1z_2 , (c) cross-correlation m_1z_1 , (d) cross-correlation m_2z_2 , (e) cross-correlation m_1z_2 , and (f) cross-correlation m_2z_1 . The two leading EOFs contribute 40.4% and 32.5%, respectively, to the total variance. The e -folding decorrelation time scales of z_1 and z_2 are 14.1 and 9.2 days, respectively. Gray shading represents 5% significance level according to the test of Bartlett (appendix).

anomalies (of Fig. 5a) have drifted poleward and project strongly onto the structure of anomalies associated with EOF2, but with an opposite sign (Figs. 5b,d; pattern correlation = -0.85). This is consistent with negative correlation of z_1z_2 when z_2 leads z_1 by 20 days (Fig. 4b).

Overall, these results suggest the existence of cross-EOF feedbacks in the propagating annular mode. In section 3, we develop a model to quantify these four feedbacks and understand the effects of their magnitude and signs on the variability (e.g., persistence) of z_1 and z_2 . But first, we will examine the variability

and characteristics of z and m in reanalysis. In particular, we will see that the z and m cross correlations in the GCM's propagating regime well resemble those in the SH reanalysis data.

b. Reanalysis

We use the 1979–2013 data from the European Centre for Medium-Range Weather Forecasts (ECMWF) interim reanalysis (ERA-Interim; Dee et al. 2011). Zonal and meridional wind components (u , v) are 6 hourly, on 1.5° latitude \times 1.5° longitude grid, and on 21 vertical levels between 1000 and 100 hPa.

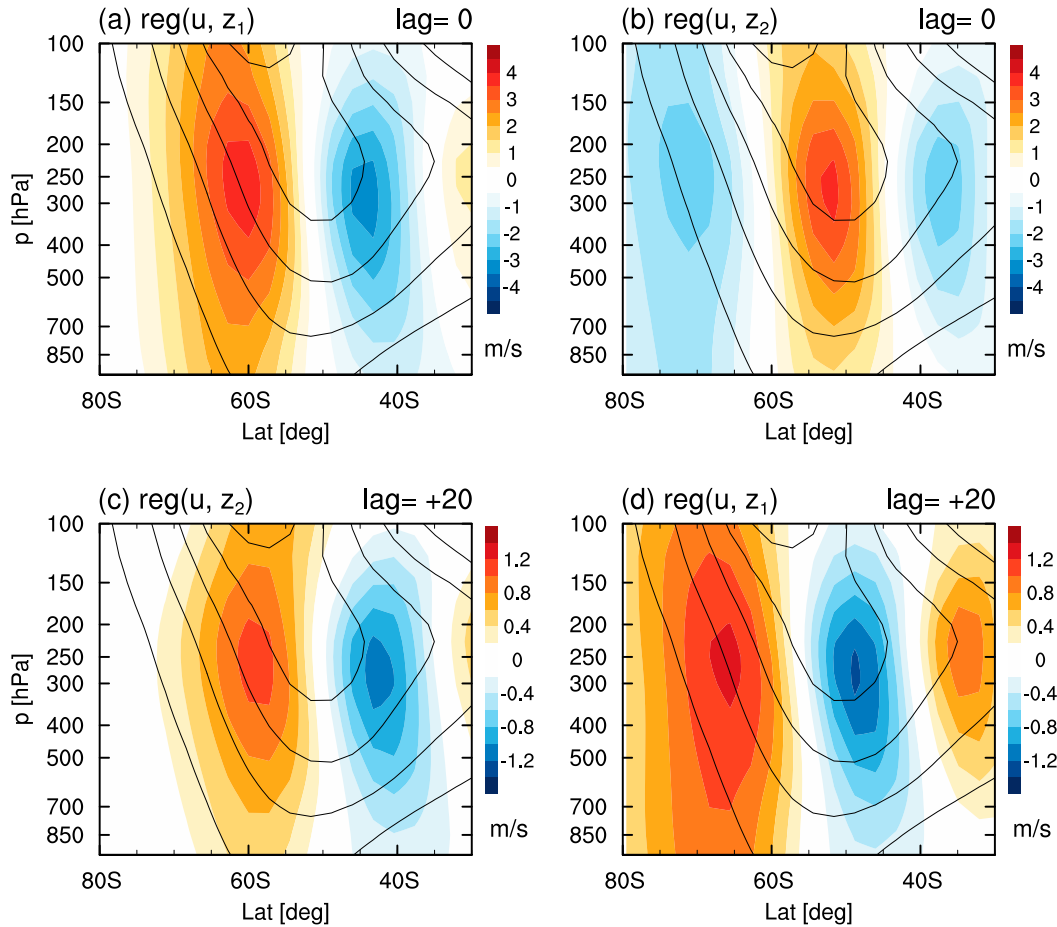


FIG. 5. Anomalous zonal-mean zonal wind (\bar{u}) regressed onto z_1 and z_2 in the GCM setup with propagating regime: (a), (b) simultaneous, (c) z_2 leads by 20 days, and (d) z_1 leads by 20 days. The contours are the climatological zonal-mean zonal wind with interval of 5 m s^{-1} .

Anomalies used for computing correlations and EOF analyses are defined as the deviations from the climatological seasonal cycle. The mean seasonal cycle is defined as the annual average and the first four Fourier harmonics of the 35-yr daily climatology.

Figure 6 shows a one-point lag-correlation map of vertically averaged zonal-mean zonal wind (\bar{u}) in the SH, where the base latitude is 30°S . Comparing this figure with Fig. 1, it can be seen that there is an indication of poleward-propagating anomalies in SH, which appear in low latitudes and migrate poleward over the course of 2–3 months (Fig. 6a). However, the poleward-propagating signals are not as evident as those observed in the GCM setup with the propagating regime (Fig. 1b or Fig. 2 of Son and Lee 2006). This is consistent with previous studies (e.g., Feldstein 1998; Feldstein and Lee 1998; Sheshadri and Plumb 2017), showing that both propagating and non-propagating anomalies exist in all seasons in the SH, which somehow obscure the propagating signals. Reconstructions based on the projections onto the two leading EOFs of zonal-mean zonal wind further show that most of the midlatitude SH wind variability can be explained by the two leading EOF modes (Fig. 6b). The ratio of the fractional variance of EOF2

(23.2%) to that of EOF1 (45.1%) is 0.51, which is right at the boundary from the rule of thumb. Overall, as already pointed out by Sheshadri and Plumb (2017), a propagating annular mode exists in the SH and is largely explained by the two leading EOF modes.

Figure 7a shows the autocorrelations of z_1 and z_2 . Consistent with LH01, the estimated decorrelation time scales of these two PCs are 10.3 and 8.1 days, respectively. Figure 7b depicts the cross-correlation $z_1 z_2$, showing statistically significant and relatively strong correlations that peak around ± 10 days. As discussed in earlier studies, such lagged correlations are a signature of the propagating annular modes (Feldstein and Lee 1998; Son and Lee 2006; Son et al. 2008; Sheshadri and Plumb 2017), implying that the period of the poleward propagation is about 20–30 days in the SH (Fig. 7b), consistent with Sheshadri and Plumb (2017) and with Fig. 6.

To understand the effects of z_1 and z_2 on m_1 and m_2 , we also examine the cross correlations between z and m at different lags (Figs. 7c–f). The shape and the magnitude of the $m_1 z_1$ and $m_2 z_2$ cross correlations (Figs. 7c,d) are similar to those originally shown by LH01 (see their Figs. 5 and 13a) and later by

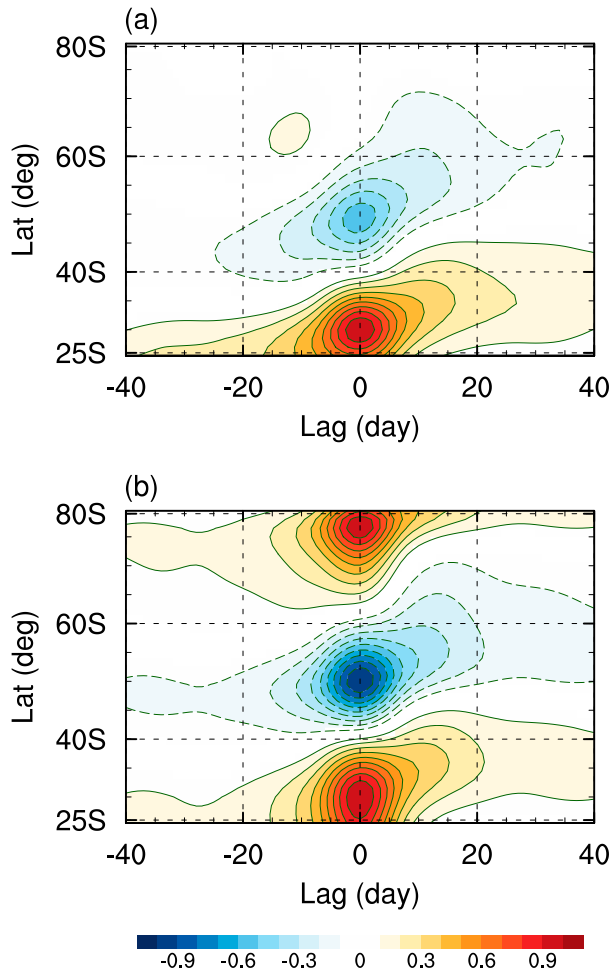


FIG. 6. One-point lag-correlation maps of the vertically averaged zonal-mean zonal wind anomalies from year-round ERA-Interim data integrated across the depth of the troposphere (1000–100 hPa) (\bar{u}) in the Southern Hemisphere. (a) Total anomaly fields and (b) reconstructed from projections onto the two leading EOFs of \bar{u} . The base latitude is at 30°S. The contour line interval is 0.1. Solid contour lines are positive, dashed contours lines are negative, and the zero contour line is omitted. Color shading denotes values significant at the 95% level according to the t test.

many others using different reanalysis products and time periods. As discussed in LH01, the statistically significant positive m_{1z_1} cross correlations at long positive lags (~ 8 –20 days) and the insignificant m_{2z_2} cross correlations for time scales longer than ~ 5 days are indicative that a positive eddy–zonal flow feedback exists only for EOF1, but not for EOF2 (also see Byrne et al. 2016; Ma et al. 2017). We emphasize that this positive feedback is from EOF1 onto itself.

To see if there are cross-EOF feedbacks, in Figs. 7e and 7f we plot the m_{1z_2} and m_{2z_1} cross correlations at different lags. The m_{1z_2} cross correlations show statistically significant positive correlations at large positive lags, signifying that a cross-EOF feedback, i.e., z_2 modifying m_1 , is present. Note that the magnitude of the m_{1z_2} cross correlations at

positive lags is overall larger than those of m_{1z_1} (Fig. 7c). There are also statistically significant but negative m_{2z_1} correlations at large positive lags, again suggesting the existence of a cross-EOF feedback, i.e., z_1 modifying m_2 . These results indicate that in the presence of the propagating regime in the SH, there are indeed cross-EOF feedbacks; however, these feedbacks were always ignored in the previous studies and reduced-order models of the SH extratropical large-scale circulation.

3. Eddy–zonal flow feedbacks in the propagating annular modes: Model and quantification

In this section, an eddy–zonal flow feedback model that accounts for the coupling of the leading two EOFs and their feedbacks, including the cross-EOF feedbacks, is introduced. Then this model is validated using synthetic data from a simple stochastic prototype, and from its analytical solution, we derive conditions for the existence of the propagating regime. Finally, we use this model to estimate the feedback strengths of the propagating annular modes in data from the reanalysis (SH) and the idealized GCMs.

a. Developing an eddy–zonal flow feedback model for propagating annular modes

With the same notations as in LH01, the time series of zonal indices (z_1 and z_2) and eddy forcing (m_1 and m_2) associated with the first two leading EOFs are calculated by projecting the vertically averaged zonal-mean zonal wind (\bar{u}) and eddy momentum flux convergence (\bar{F}) anomalies onto the patterns of the first and second EOFs of \bar{u} [see Eqs. (1) and (2)]. Equations for the tendency of z_1 and z_2 can be then formulated as

$$\frac{dz_1}{dt} = m_1 - \frac{z_1}{\tau_1}, \quad (4)$$

$$\frac{dz_2}{dt} = m_2 - \frac{z_2}{\tau_2}, \quad (5)$$

where t is time and the last term on the right-hand side in each equation represents damping (mainly due to surface friction) with time-scale τ . As discussed in LH01, Eqs. (4) and (5) can be interpreted as the zonally and vertically averaged zonal momentum equation

$$\frac{\partial \bar{u}}{\partial t} = -\frac{1}{\cos^2 \phi} \frac{\partial (\langle \bar{u} \bar{v} \cos^2 \phi \rangle)}{\partial \phi} - D, \quad (6)$$

projected onto EOF1 and EOF2, respectively. In the above equation, D includes the effects of surface drag and is modeled as Rayleigh drag in Eqs. (4) and (5).

Assuming a linear representation for the feedback of an EOF onto itself, LH01 and later studies wrote $m_1(t) = \tilde{m}_1(t) + b_1 z_1(t)$ and $m_2(t) = \tilde{m}_2(t) + b_2 z_2(t)$, where b_1 and b_2 are the feedback strengths and are assumed to be independent of z and t . A value of $b_j > 0$ implies a positive feedback that prolongs the persistence of z_j ; \tilde{m}_j is the random, zonal flow-independent component of the eddy forcing that drives the high-frequency variability of z_j (LH01; Ma et al. 2017).

Here, to account for the cross-EOF feedbacks, i.e., the effect of z_2 on m_1 and z_1 on m_2 , we extend the LH01 model and write

$$m_1 = \tilde{m}_1 + b_{11}z_1 + b_{12}z_2, \quad (7)$$

$$m_2 = \tilde{m}_2 + b_{21}z_1 + b_{22}z_2. \quad (8)$$

With $j, k = 1, 2$, b_{jk} is the strength of the linearized feedback of z_k onto z_j through modifying m_j in the quasi-steady limit. Thus, the cross-EOF feedbacks are represented by the terms involving b_{12} and b_{21} . To find the values of b_{jk} , we can use the lagged-regression method of Simpson et al. (2013), which assumes that $\text{reg}_l(\tilde{m}_j, z_j) = \text{sum}[\tilde{m}_j(t+l)z_j(t)] \approx 0$ at large positive lags l (i.e., longer than eddy lifetime).² By lag regressing each term in Eq. (7) onto z_1 and then onto z_2 , we find

$$\begin{bmatrix} \text{reg}_l(z_1, z_1) & \text{reg}_l(z_2, z_1) \\ \text{reg}_l(z_1, z_2) & \text{reg}_l(z_2, z_2) \end{bmatrix} \begin{bmatrix} b_{11} \\ b_{12} \end{bmatrix} = \begin{bmatrix} \text{reg}_l(m_1, z_1) \\ \text{reg}_l(m_1, z_2) \end{bmatrix}, \quad (9)$$

and similarly, from Eq. (8) we find

$$\begin{bmatrix} \text{reg}_l(z_2, z_1) & \text{reg}_l(z_1, z_1) \\ \text{reg}_l(z_2, z_2) & \text{reg}_l(z_1, z_2) \end{bmatrix} \begin{bmatrix} b_{21} \\ b_{22} \end{bmatrix} = \begin{bmatrix} \text{reg}_l(m_2, z_1) \\ \text{reg}_l(m_2, z_2) \end{bmatrix}, \quad (10)$$

where we have assumed $\text{reg}_l(\tilde{m}_j, z_k) \approx 0$ for $j, k = 1, 2$.

Note that if one attempts to find b_{11} using a single-EOF approach such as LH01, then, from Eq. (7), one would be implicitly assuming that $\text{reg}_l(m_1 - b_{11}z_1, z_1) = \text{reg}_l(\tilde{m}_1 + b_{12}z_2, z_1) = \text{reg}_l(\tilde{m}_1, z_1) + b_{12}\text{reg}_l(z_2, z_1) \approx b_{12}\text{reg}_l(z_2, z_1)$ is zero. However, as shown earlier, in the propagating regime, the z_1z_2 cross correlations can be large at long lags, and as discussed below, the range of time lags needed to be used in Eqs. (9) and (10) and the lags at which z_1z_2 cross correlations peak are often comparable. Consequently, if $b_{12} \neq 0$, the key assumption of the statistical methods developed to quantify eddy–zonal flow feedbacks, i.e., that $m_1 - b_{11}z_1$ is random and independent of the jet (LH01; Simpson et al. 2013; Ma et al. 2017) is violated. Therefore, b_{jk} should be determined together by solving the systems of Eqs. (9) and (10).

The basic assumptions of our model, Eqs. (4)–(10), are similar to those of the LH01 model: (i) a linear representation of the feedbacks is sufficient, and (ii) the eddy forcing m does not have long-term memory independent of the variability in the jet (represented by z_1 and z_2). The second assumption means that at sufficiently large positive lags (beyond the time scales over which there is significant autocorrelation in \tilde{m}) the feedback component of the eddy forcing will dominate the m_jz_k cross correlations (LH01; Chen and Plumb 2009; Simpson et al. 2013; Ma et al. 2017), i.e., $\text{reg}_l(\tilde{m}_j, z_k) \approx 0$ at “large-enough” positive lags. Note that one cannot use a lag that is too long because then even $\text{reg}_l(z_j, z_j)$ would be small and

inaccurate. To find the appropriate lag to use, one must look for nonzero m_jz_k cross correlations at positive lags beyond an eddy lifetime. In this study, the strengths of the individual feedbacks are averaged over positive lags of 8–20 days for both GCM and reanalysis (e.g., Simpson et al. 2013; Burrows et al. 2016). We choose this range in order to avoid the high-frequency variability at short lags (indicated by impulsive and oscillatory characters of the \tilde{m} autocorrelation) and strong damping at the very long lags.

In the following section, we will present a proof of concept for this eddy–zonal flow feedback model using synthetic data obtained from a simple stochastic prototype and show that using Eqs. (9) and (10), the prescribed feedbacks can be accurately backed out.

b. Validation using synthetic data from a simple stochastic prototype

We begin by constructing a simple stochastic system to produce synthetic time series z and m in the presence or absence of cross-EOF feedbacks. The equations of this system are the same as Eqs. (4) and (5) and (7) and (8). Following Simpson et al. (2013), we generate a synthetic time series of the random component of the eddy forcing $\tilde{m}_{1,2}$ using a second-order autoregressive (AR2) noise process:

$$\tilde{m}_1(t) = 0.6\tilde{m}_1(t-2) - 0.3\tilde{m}_1(t-1) + \varepsilon_1(t), \quad (11)$$

$$\tilde{m}_2(t) = 0.6\tilde{m}_2(t-2) - 0.3\tilde{m}_2(t-1) + \varepsilon_2(t), \quad (12)$$

where t denotes time (in days) and ε is white noise distributed uniformly between -1 and $+1$.

Synthetic time series of z_1, z_2, m_1 , and m_2 are produced by numerically integrating Eqs. (4) and (5), (7) and (8), and (11) and (12) forward in time with two different sets of prescribed b_{11}, b_{22}, b_{12} , and b_{21} . In the first set, $b_{12} > 0, b_{22} = 0$, and there is no cross-EOF feedback, i.e., $b_{12} = b_{21} = 0$ (Table 3). In the second set, b_{11} and b_{22} are the same as those in the first set, but here, there is cross-EOF feedback, i.e., b_{12} and $b_{21} \neq 0$ (Table 3). For both sets, we use $\tau_1 = \tau_2 = 8$ days. The values of b and τ are reasonably chosen based on the observed values in the SH (see Table 4).

Spectral analysis of $z_{1,2}$ and $m_{1,2}$ shows that the synthetic data indeed have characteristics similar to those of the observed SH. For example, for the case with cross feedbacks (Fig. 8), we find that consistent with observations [see Fig. 4 of LH01 or Fig. 3 of Ma et al. (2017)], the time scales of z_1 and z_2 are much longer (i.e., slower variability) than m_1 and m_2 , and the power spectra of z can be interpreted, to the first order, as reddening of the power spectra of eddy forcing m (LH01; Ma et al. 2017). The power spectra of eddy forcings m_1 and m_2 have in general broad maxima centered at the synoptic frequency (with m_1 also peaking at low frequency), consistent with observations. Given that the characteristics of the synthetic data mimic the key characteristics of the observed annular modes, we use this idealized framework to validate the lagged-correlation approach of Eqs. (9) and (10) for quantifying eddy–zonal flow feedbacks.

Figure 9 shows the lagged-correlation analysis of the synthetic data without cross-EOF feedbacks. It is clearly seen that

² Note that in general, for any two time series $x(t)$ and $y(t)$ and a given time lag l , we have defined $\text{reg}_l[x(t), y(t)] = \text{sum}[x(t+l)y(t)]$ where the summation is over time (i.e., regression). Later in the paper, when a range is given for l , we mean that following Simpson et al. (2013), reg_l is computed for each l and then averaged over that range.

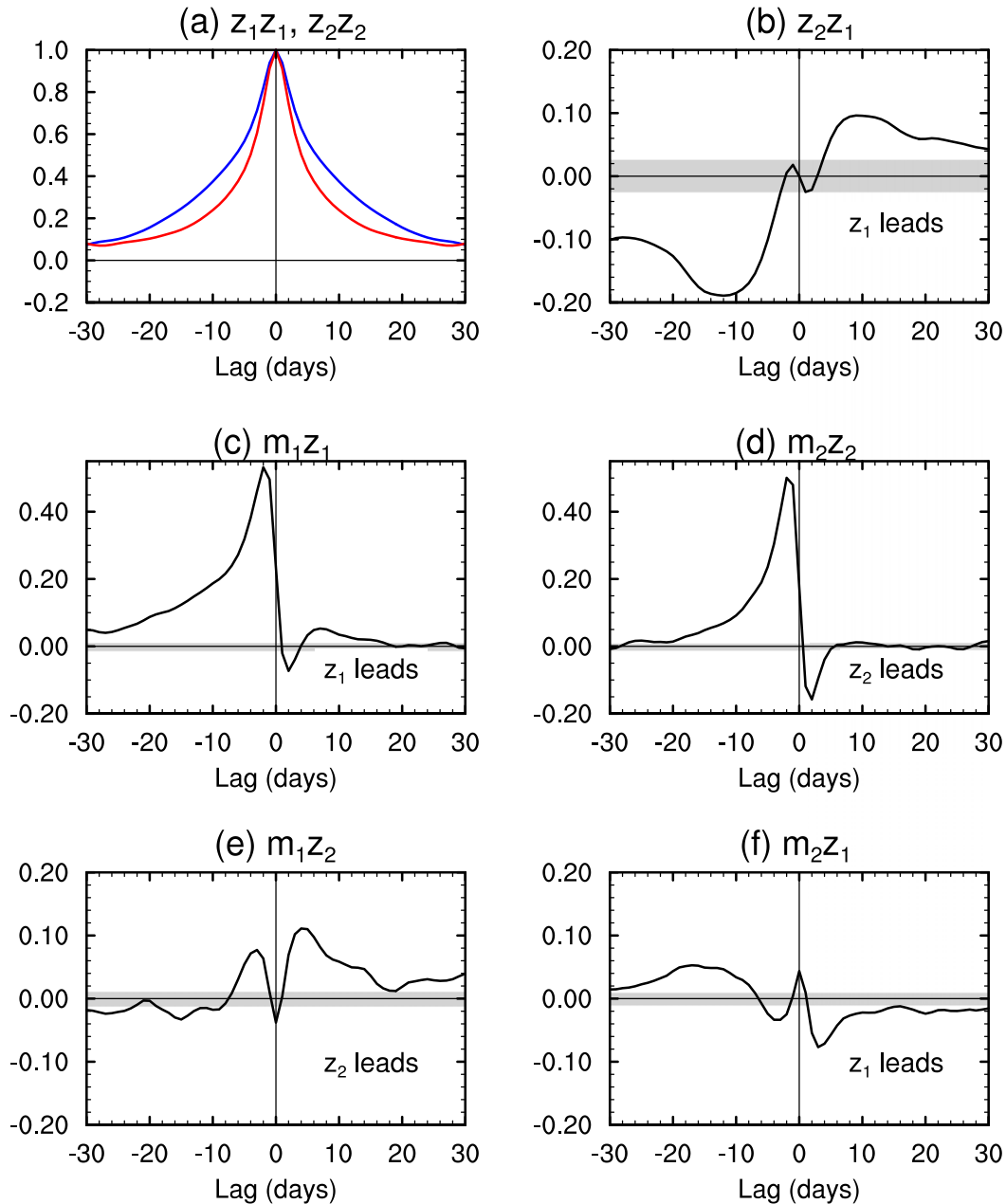


FIG. 7. Lagged-correlation analysis for the Southern Hemisphere, calculated from year-round ERA-Interim data. (a) Autocorrelations of z_1 (blue) and z_2 (red), (b) cross-correlation $z_1 z_2$, (c) cross-correlation $m_1 z_1$, (d) cross-correlation $m_2 z_2$, (e) cross-correlation $m_1 z_2$, and (f) cross-correlation $m_2 z_1$ at different lags. The two leading EOFs contribute to 45.1% and 23.2% of the total variance, respectively. The e -folding decorrelation time scales of z_1 and z_2 are 10.3 and 8.1 days, respectively. Gray shading represents 5% significance level according to the test of Bartlett (appendix).

the only noticeable cross correlations are that of $m_1 z_1$, and there are no (statistically significant) cross correlations between $z_1 z_2$, $m_1 z_2$ and $m_2 z_1$ at any lag, consistent with a non-propagating regime and the absence of cross-EOF feedbacks (Fig. 2). Using Eqs. (9) and (10) and lag $l = 8$ –20 days, we can closely estimate the prescribed feedback parameters, i.e., $b_{11} = 0.04 \text{ day}^{-1}$ and $b_{22} = b_{12} = b_{21} = 0$ (see Table 3).

Figure 10 shows the lagged-correlation analysis of the synthetic data with cross-EOF feedbacks. First, we see that there are statistically significant and often large cross correlations in $z_1 z_2$, $m_1 z_1$, $m_1 z_2$, and $m_2 z_1$, with the shape of the cross-correlation distributions not that different from that of the SH reanalysis and the idealized GCM setup with propagating regime (Figs. 4 and 7). The positive $m_1 z_1$ and near zero $m_2 z_2$ cross correlations at large positive

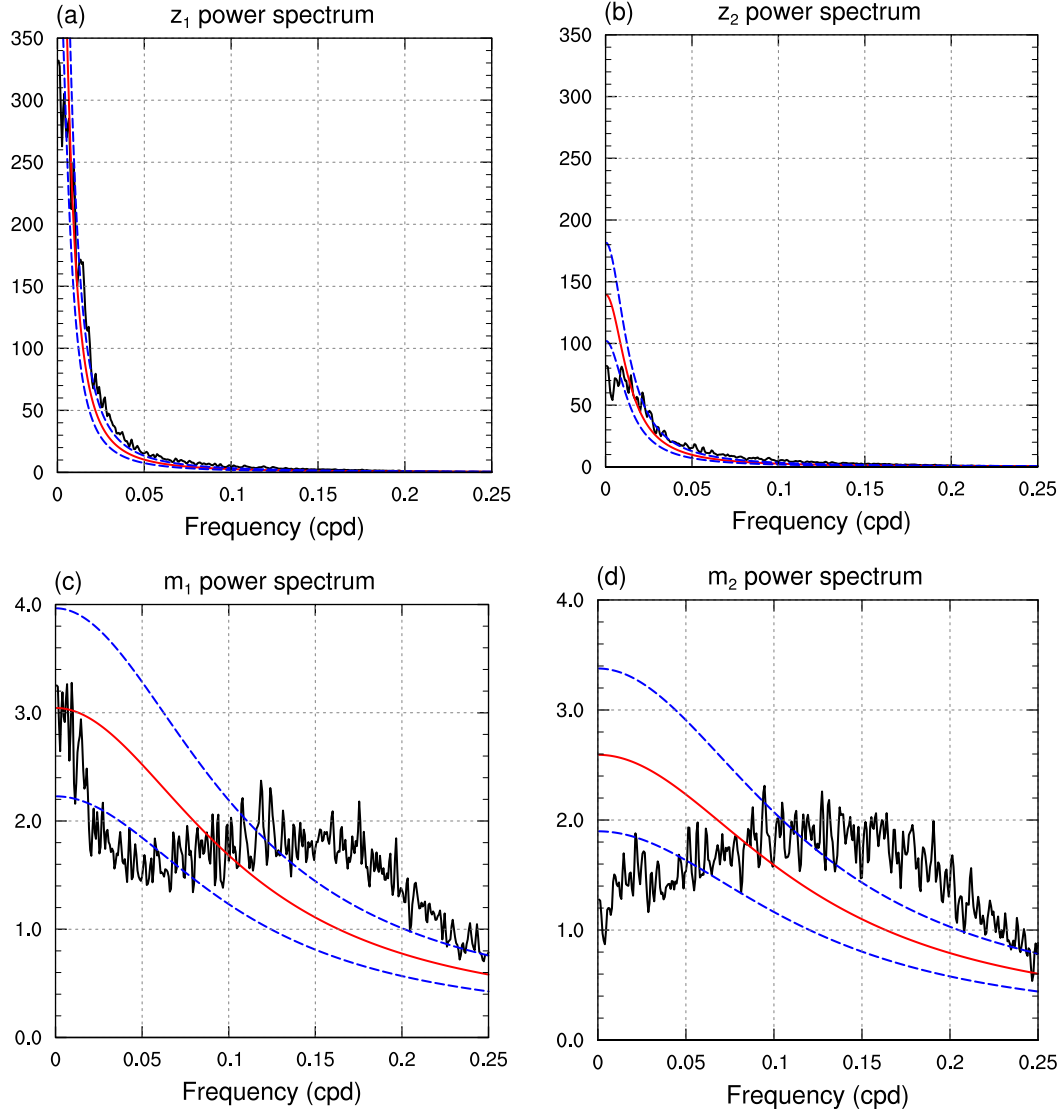


FIG. 8. Spectra of $z_{1,2}$ and $m_{1,2}$ from the synthetic data with cross-EOF feedbacks. Black lines show the power spectra of (a) z_1 , (b) z_2 , (c) m_1 , and (d) m_2 . The red-noise spectra are indicated by the smooth solid red curves, and the smooth dashed blue lines are the 5% and 95% a priori confidence limits.

lags signify a positive z_1 -onto- z_1 feedback through m_1 , but no z_2 -onto- z_2 feedback through m_2 , consistent with the prescribed $b_{11} > 0$ and $b_{22} = 0$. In addition, Figs. 10e and 10f also show that there are statistically significant and large correlations in $m_1 z_2$ and $m_2 z_1$ at positive lags, consistent with the introduction of cross-EOF feedbacks by setting $b_{12} = 0.06 \text{ day}^{-1}$ and $b_{21} = -0.025 \text{ day}^{-1}$. The positive $m_1 z_2$ cross correlations at positive lags are higher than those of $m_1 z_1$ (note that $b_{12}/b_{11} \approx 1.5$), and the sign of $m_2 z_1$ cross correlations is opposite to the sign of $m_1 z_2$ cross correlations (note that $b_{12}b_{21} < 0$). Using Eqs. (9) and (10) and lag $l = 8\text{--}20$ days, we can again closely estimate the prescribed feedback parameters, including the strength of the cross-EOF feedbacks (see Table 3).

The above analyses validate the approach using Eqs. (9) and (10) for quantifying the feedback strengths b_{jk} in data from both propagating and nonpropagating regimes. Furthermore, a

closer examination of z_1 and z_2 autocorrelations in Figs. 9a and 10a show that both z_1 and z_2 in the case without cross-EOF feedbacks are more persistent than those in the case with cross-EOF feedbacks; e.g., the e -folding decorrelation time scale of z_1 is 18.6 days in Fig. 9a while it is 13.9 days in Fig. 10a. This observation might be counterintuitive because both cases have the same $b_{11} > 0$ while the case with cross-EOFs feedback has $b_{12} > 0$, which might seem like another positive feedback that should further prolong the persistence of z_1 . Finally, we notice that $b_{12}b_{21} < 0$ in Table 3 and in the SH reanalysis and idealized GCM setup with the propagating regime (Tables 4 and 5). Synthetic data generated with the same parameters as in Table 2 but with the sign of b_{21} flipped results in cross-correlation distributions that are vastly different from those of Fig. 10 and what is seen in the SH reanalysis

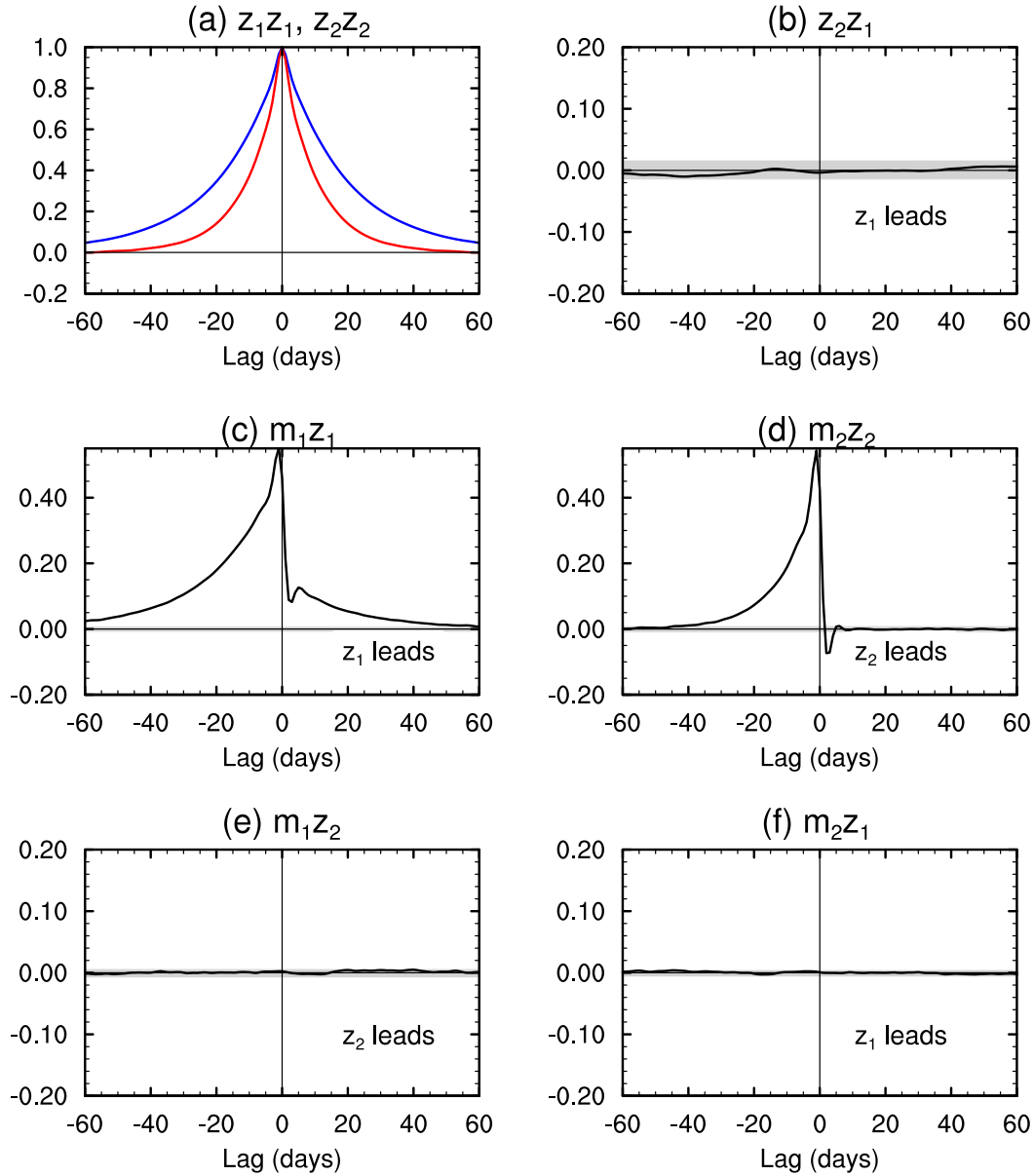


FIG. 9. Lagged-correlation analysis of synthetic data without cross-EOF feedbacks. (a) Autocorrelation of z_1 (blue) and z_2 (red), (b) cross-correlation z_1z_2 , (c) cross-correlation m_1z_1 , (d) cross-correlation m_2z_2 , (e) cross-correlation m_1z_2 , and (f) cross-correlation m_2z_1 . The e -folding decorrelation time scales of z_1 and z_2 are 18.6 and 9.2 days, respectively. Gray shading represents 5% significance level according to the test of Bartlett ([appendix](#)).

and idealized GCM. Inspired by these observations, next we examine the analytical solution of the deterministic version of Eqs. (4) and (5) and Eqs. (7) and (8) to better understand the impacts of the strength and sign of b_{jk} on the variability and in particular the persistence of z_1 and z_2 .

c. Analytical solution of the two-EOF eddy–zonal flow feedback model

We focus on the deterministic (i.e., $\tilde{m}_j = 0$) version of Eqs. (4) and (5) and Eqs. (7) and (8), which can be rewritten as the following system of ordinary differential equations (ODEs):

$$\dot{\mathbf{z}} = \mathbf{A}\mathbf{z}, \quad (13)$$

where

$$\mathbf{z} = \begin{bmatrix} z_1 \\ z_2 \end{bmatrix} \quad \text{and} \quad \mathbf{A} = \begin{bmatrix} b_{11} - \frac{1}{\tau_1} & b_{12} \\ b_{21} & b_{22} - \frac{1}{\tau_2} \end{bmatrix}. \quad (14)$$

The solution to this system is

$$\mathbf{z}(t) = e^{\mathbf{A}t} \mathbf{z}(0) = [\mathbf{V} e^{\mathbf{\Lambda}t} \mathbf{V}^{-1}] \mathbf{z}(0), \quad (15)$$

where \mathbf{V} and $\mathbf{\Lambda}$ are the eigenvector and eigenvalue matrices of \mathbf{A} :

$$\mathbf{V} = [\mathbf{v}_1 \ \mathbf{v}_2] = \begin{bmatrix} v_{11} & v_{12} \\ v_{21} & v_{22} \end{bmatrix} \quad \text{and} \quad \mathbf{\Lambda} = \begin{bmatrix} \lambda_1 & 0 \\ 0 & \lambda_2 \end{bmatrix}. \quad (16)$$

To find the eigenvalues λ , we set the determinant of \mathbf{A} equal to zero and solve the resulting quadratic equation to obtain

$$\lambda_{1,2} = -\frac{1}{2} \left(\frac{1}{\tau_1} + \frac{1}{\tau_2} - b_{11} - b_{22} \right) \pm \frac{1}{2} \sqrt{\left\{ \left(\frac{1}{\tau_1} - \frac{1}{\tau_2} \right) - (b_{11} - b_{22}) \right\}^2 + 4b_{12}b_{21}}, \quad (17)$$

which, in the limit of $\tau_1 \approx \tau_2$ (reasonable given their estimated values in [Tables 4](#) and [5](#)), simplifies to

$$\lambda_{1,2} = -\frac{1}{2} \left(\frac{2}{\tau} - b_{11} - b_{22} \right) \pm \frac{1}{2} \sqrt{(b_{11} - b_{22})^2 + 4b_{12}b_{21}}. \quad (18)$$

The solution [Eq. (15)] can be rewritten as

$$\mathbf{z} = c_1 e^{\lambda_1 t} \mathbf{v}_1 + c_2 e^{\lambda_2 t} \mathbf{v}_2, \quad (19)$$

where c_1 and c_2 depend on the initial condition.

This system has a decaying-oscillatory solution, i.e., is in the propagating regime, if and only if the eigenvalues (18) have nonzero imaginary parts, which requires, as a necessary and sufficient condition,

$$(b_{11} - b_{22})^2 < -4b_{12}b_{21}. \quad (20)$$

Equation (20) also implies that a necessary condition for the existence of propagating regimes is

$$b_{12}b_{21} < 0. \quad (21)$$

Thus, nonzero cross-EOF feedbacks of opposite signs are essential components of the propagating regime dynamics. The propagating regimes in the stochastic prototype ([Table 2](#)), SH reanalysis ([Table 4](#)), and idealized GCM ([Table 5](#)) satisfy the conditions of Eqs. (20) and (21), while the nonpropagating regimes ([Tables 1](#) and [5](#)) do not.

In the nonpropagating regime, $\lambda_{1,2} = -\sigma_{1,2} < 0$ and $\mathbf{v}_{1,2}$ are real and in this regime, $z_{1,2}$ just decays exponentially according to

$$\mathbf{z} = c_1 e^{(-\sigma_1 t)} \mathbf{v}_1 + c_2 e^{(-\sigma_2 t)} \mathbf{v}_2. \quad (22)$$

In the propagating regime, $\lambda_{1,2} = -\sigma \pm i\omega$ and $\mathbf{v}_{1,2}$ are complex where

$$\sigma = \frac{1}{2} \left(\frac{1}{\tau_1} + \frac{1}{\tau_2} - b_{11} - b_{22} \right), \quad (23)$$

$$\omega = \frac{1}{2} \sqrt{\left\{ \left(\frac{1}{\tau_1} - \frac{1}{\tau_2} \right) - (b_{11} - b_{22}) \right\}^2 + 4b_{12}b_{21}}. \quad (24)$$

In this regime, $z_{1,2}$ decay and oscillate according to

$$\mathbf{z} = c_1 e^{(-\sigma t)} e^{(i\omega t)} \mathbf{v}_1 + c_2 e^{(-\sigma t)} e^{(-i\omega t)} \mathbf{v}_2. \quad (25)$$

Realizing that in this case $v_{11} = v_{12}$ are real, and $v_{21} = v_{22}^*$ and $c_1 = c_2^* = c$, where the asterisk means complex conjugate, we can rewrite the above equations as

$$z_1 = [c e^{(i\omega t)} v_{11} + c^* e^{(-i\omega t)} v_{11}] e^{(-\sigma t)}, \quad (26)$$

$$z_2 = [c e^{(i\omega t)} v_{22}^* + c^* e^{(-i\omega t)} v_{22}] e^{(-\sigma t)}. \quad (27)$$

These equations show that z_1 and z_2 have the same decay rate (σ) but different oscillatory components with frequency ω . These results are consistent with the POP analysis of [Sheshadri and Plumb \(2017\)](#), who showed that EOF1 and EOF2 are, respectively, the real and imaginary parts of a single decaying-oscillatory POP mode (see their section 4b). As a result, the two modes have the same decay rate and frequency, but have different autocorrelation function decay rates and have strong lag cross correlations because the oscillations are out of phase. A key contribution of our work is to find the decay rate σ and frequency ω as a function of b_{jk} and τ_j [Eqs. (23) and (24)].

To understand the effects of the feedback strength b_{jk} on the persistence of z_j , we compute the analytical solutions for 5 systems that have the same $b_{11} > 0$ and $b_{22} = 0$ ([Table 3](#)): in EXP1, there is no cross-EOF feedback ($b_{12} = b_{21} = 0$), while in EXP2–EXP5, $b_{12} > 0$ and $b_{21} < 0$ and they have been doubled from experiment to experiment. [Figure 11](#) shows the autocorrelation coefficients of z_1 and their e -folding decorrelation time scales for EXP1–EXP5. EXP1, corresponding to nonpropagating regimes, has the slowest-decaying autocorrelation function, i.e., longest e -folding decorrelation time scale ([Figs. 11a,b](#)). EXP2–EXP5, which all satisfy the condition of Eq. (20), have faster-decaying autocorrelation functions, i.e., shorter e -folding decorrelation time scale, consistent with our earlier results in idealized GCM and stochastic prototype ([Figs. 4](#) and [10](#)). As discussed above, in the propagating regime, the eigenvectors and the corresponding eigenvalues are complex and thus, $z_{1,2}$ do not decay just exponentially, but rather show some oscillatory characteristics too [[Fig. 11a](#), Eqs. (26) and (27)]. Since the frequency of these oscillations ω [Eq. (24)] increases as the cross-EOF feedback strengths increase, shorter time scales in z_1 are expected in the experiment with stronger $b_{12}b_{21}$ ([Fig. 11b](#)).

The dependence of the e -folding decorrelation time scales of z_1 and z_2 on the feedback strengths, and in particular the cross-EOF feedback strengths, is further evaluated in [Fig. 12](#). In [Fig. 12a](#), it is clearly seen that the impact of increasing $b_{11} > 0$ in the propagating regime (filled symbols) is to increase the persistence, i.e., decorrelation time scale, of z_1 , consistent with increasing the positive eddy–zonal flow feedback (z_1 -onto- z_1 through m_1). However, when the feedback is further increased to twice the control value, the condition of Eq. (20) for the existence of a decaying-oscillatory solution is not satisfied anymore, and consistent with this, we see that the system undergoes a transition to the nonpropagating regime. Further increasing b_{11} leads to substantially more

persistent z_1 and less persistence z_2 . Note that in non-propagating regimes when $b_{12}b_{21} \neq 0$, the decay of z_2 depends on b_{11} too [see Eq. (18)].

Figure 12b shows that in the propagating regime, unlike increasing $b_{11} > 0$, increasing $b_{12} > 0$ leads to reduction in the persistence of z_1 . This is the counterintuitive behavior we had observed earlier in the stochastic prototype (section 3b). Now we understand that this is because increasing b_{12} increases the frequency of the oscillation ω [Eq. (24)] in the system, resulting in reduction in the decorrelation time scale of z_1 (and z_2); also see Fig. 11. Such impact can even be more pronounced when both cross-EOF feedbacks b_{12} and b_{21} are increased (Fig. 12c), leading to shorter decorrelation time scales. Because a positive b_{12} decreases the persistence of z_1 , we do not refer to it as a “positive feedback.” To understand this behavior, we have to keep in mind that in the eddy forcing of z_1 (z_2), i.e., m_1 in Eq. (7) [m_2 in Eq. (8)], $b_{12} > 0$ ($b_{21} < 0$) is the coefficient of z_2 (z_1). When z_2 leads z_1 , they are negatively correlated (Figs. 4b, 7b, and 10b), thus z_2 multiplied by $b_{12} > 0$ reduces m_1 that is forcing z_1 , decreasing the persistence of z_1 . Similarly, when z_1 leads z_2 , they are positively correlated, thus z_1 multiplied by $b_{21} < 0$ reduces m_2 and thus the persistence of z_2 .

Finally, for the sake of completeness, we also examine the effect of increasing b_{11} in the absence of cross-EOF feedback (Fig. 12d). As expected, increasing b_{11} leads to increasing the persistence of z_1 and has no impact on the persistence of z_2 as now z_1 and z_2 are completely decoupled.

d. Quantifying eddy–zonal flow feedbacks in reanalysis and idealized GCM

The results of sections 3b and 3c show the importance of carefully quantifying and interpreting the eddy–zonal flow feedbacks, including the cross-EOF feedbacks, to understand the variability of the zonal-mean flow.

Table 4 presents the feedback strengths obtained from applying (9) and (10) with $l = 8$ –20 days to the year-round SH reanalysis data. We find $b_{11} = 0.038 \text{ day}^{-1}$, a positive feedback from z_1 onto z_1 , consistent with the findings of LH01 in their pioneering work. This estimate of b_{11} is slightly higher than what we find using the single-EOF approach ($b_{11} = 0.035 \text{ day}^{-1}$), which is the same as what LH01 found using their spectral cross-correlation method. We also find nonzero cross-EOF feedbacks: $b_{12} = 0.059 \text{ day}^{-1}$ and $b_{21} = -0.020 \text{ day}^{-1}$. We estimate $b_{22} = 0.017 \text{ day}^{-1}$, which is slightly higher from what the single-EOF approach yields (Table 4). The estimated feedback strengths and friction rates (τ) in Table 4 satisfy the condition for the propagating regime [Eq. (20)]. It should be noted that we also extended our approach to include the leading 3 EOFs and quantified the 9 feedback strengths; however, we found the effects of EOF3 on EOF1 and EOF2 negligible, which suggests that a two-EOF model [Eqs. (9) and (10)] is enough to describe the current SH extratropical large-scale circulation (not shown).

Table 5 presents the feedback strengths obtained from applying (9) and (10) with $l = 8$ –20 days to the two setups of the idealized GCM. In the nonpropagating regime, we find $b_{11} = 0.133 \text{ day}^{-1}$, and small b_{22} and negligible b_{12} and b_{21} , indicating

the absence of cross-EOF feedbacks, consistent with insignificant m_1z_2 and m_2z_1 cross correlations (Figs. 2e,f). The values of b_{jk} do not satisfy the condition for propagating regime, which is consistent with weak cross correlation between z_1 and z_2 at long lags (Fig. 2b). These results suggest that a strong z_1 -onto- z_1 feedback dominates the dynamics of the annular mode in this setup (the standard Held–Suarez configuration), which leads to an unrealistically persistent annular mode, similar to what is seen in Fig. 12d, and consistent with the findings of previous studies (Son and Lee 2006; Son et al. 2008; Ma et al. 2017). Using the linear response function (LRF) of this setup computed by Hassanzadeh and Kuang (2016a, 2019) showed that this eddy–zonal flow feedback is due to enhanced low-level baroclinicity [as proposed by Robinson (2000) and LH01] and estimated, from a potential vorticity budget analysis, that the positive feedback is increasing the persistence of the annular mode by a factor of 2.

In the propagating regime, we find $b_{11} = 0.101 \text{ day}^{-1}$, which is slightly lower than b_{11} of the nonpropagating regime. However, in the propagating regime, we also find strong cross-EOF feedbacks $b_{12} = 0.075 \text{ day}^{-1}$, $b_{21} = -0.043 \text{ day}^{-1}$ as well as $b_{22} = 0.023 \text{ day}^{-1}$. These feedback strengths satisfy the condition for the propagating regime, consistent with strong cross correlation between z_1 and z_2 at long lags (Fig. 4b). Comparing the two rows of Table 5 and Figs. 2a and 4a with Table 4 and Fig. 7a suggests that while it is true that the b_{11} of the idealized GCM’s nonpropagating regime is larger than that of the SH reanalysis (by a factor of 3.5), the unrealistic persistence of z_1 in this setup (time scale ≈ 65 days) compared to that of the reanalysis (time scale ≈ 10 days; compare Figs. 2a and 7a) could be, at least partially, due to the absence of cross-EOF feedbacks (thus oscillations). As we showed earlier in section 3c, these oscillations reduce the persistence of the annular modes. The GCM setup with propagating regime has b_{11} that is around 2.7 times larger than that of the SH reanalysis, yet their z_1 e -folding decorrelation time scales are comparable (14 days vs 10 days).

Note that like past studies, we have used the e -folding decorrelation time scale of z_1 as the main measure of the time scale of the annular modes (e.g., Gerber et al. 2008b; Sheshadri and Plumb 2017; Ma et al. 2017). The e -folding decorrelation time scale of z_1 measures how long an anomalous structure stays the same (with respect to the stationary pattern of EOF1), which is an appropriate measure of lifetime for the nonpropagating annular modes. However, for the propagating annular modes, in which anomalies propagate but may not change in structure and amplitude, a better measure of lifetime might be needed. We suggest that the one-point lag-correlation maps (Figs. 1 and 6) can provide one example of such measure. For instance, we can track the contour line of -0.4 correlation in Fig. 1b, which spans lag day -35 to lag day $+25$. This suggests a lifetime of around 60 days for anomalies that propagate poleward and remain anticorrelated with an anomalous structure at the base latitude of 30°S with a magnitude of 0.4 or higher [we choose 0.4, motivated by $\exp(-1) \approx 0.37$, but other cutoff values could be used too]. Applying the same definition of lifetime to the nonpropagating regime (Fig. 1a) yields ~ 100 days. Similar analysis of the year-round

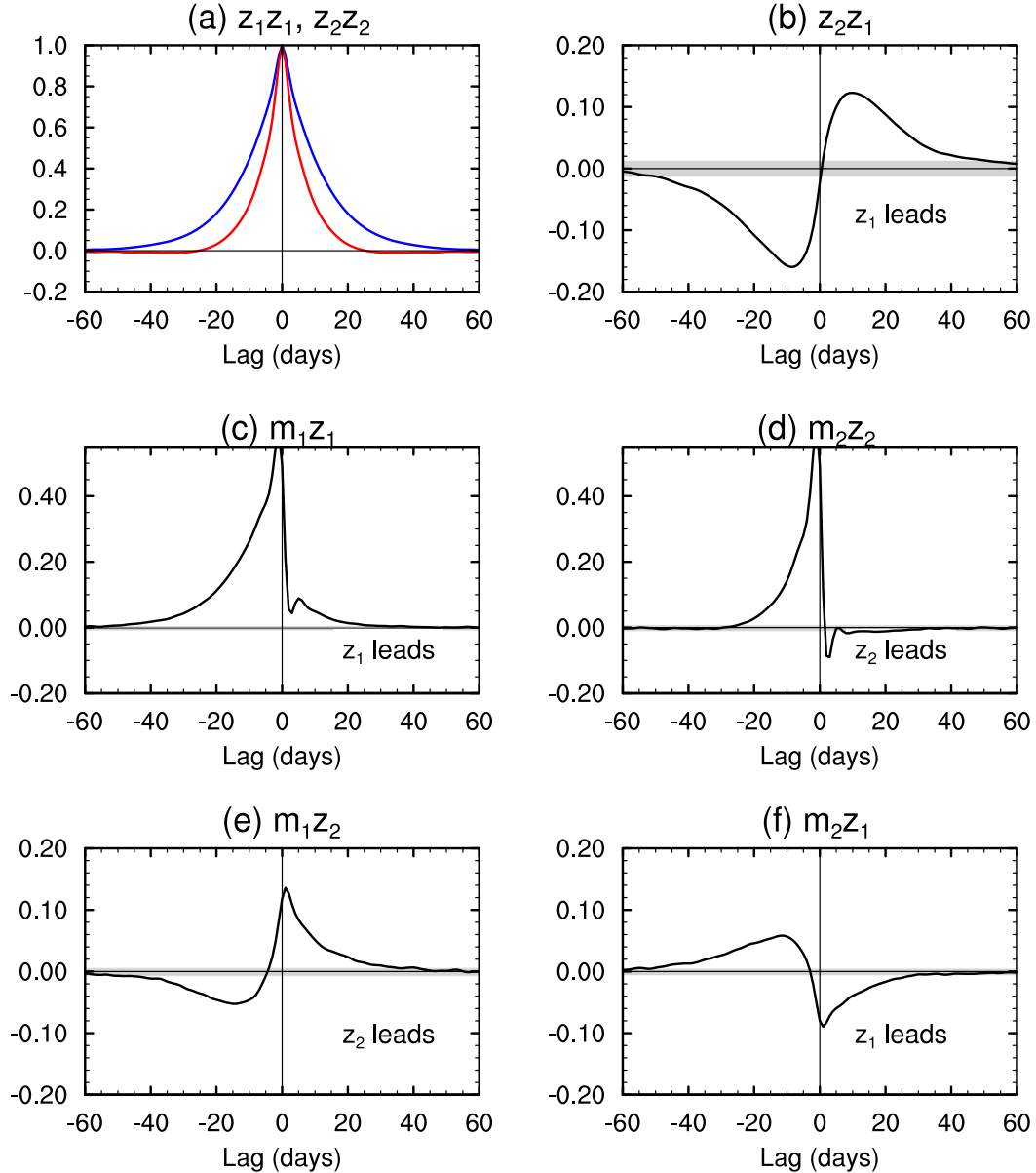


FIG. 10. Lagged-correlation analysis of synthetic data with cross-EOF feedbacks. (a) Autocorrelation of z_1 (blue) and z_2 (red), (b) cross-correlation z_1z_2 , (c) cross-correlation m_1z_1 , (d) cross-correlation m_2z_2 , (e) cross-correlation m_1z_2 , and (f) cross-correlation m_2z_1 . The e -folding decorrelation time scales of z_1 and z_2 are 13.9 and 6.5 days, respectively. The regions outside the gray shading indicate 95% significance level according to the test of Bartlett (appendix).

ERA-Interim data (Fig. 6b) suggests a lifetime of around 20 days for the propagating anomalies. The similarity between the decorrelation time scales of the reanalysis and GCM's propagating regime and the substantial difference between the lifetime of propagating anomalies in these two systems (at least based on one-point lag-correlation maps) suggest that future studies should carefully examine different measures of time scale for the propagating regimes.

In summary, these findings show the importance of quantifying and examining cross-EOF feedbacks to fully understand the dynamics and variability of the annular modes and to better

evaluate how well the GCMs simulate the extratropical large-scale circulation.

TABLE 1. Prescribed and estimated feedback strengths (day^{-1}) in synthetic data for the case without cross-EOF feedbacks. The imposed damping rates of friction are $\tau_1 = \tau_2 = 8$ days. The values of b and τ are motivated by the observed ones; see Table 4.

Feedback	b_{11}	b_{12}	b_{21}	b_{22}
Prescribed	0.040	0.000	0.000	0.000
Estimated [Eqs. (9) and (10)]	0.042	0.001	−0.0006	0.0005

TABLE 2. Prescribed and estimated feedback strengths (day^{-1}) in synthetic data for the case with cross-EOF feedbacks. The imposed damping rates of friction are $\tau_1 = \tau_2 = 8$ days. The values of b and τ are motivated by the observed ones; see Table 4.

Feedback	b_{11}	b_{12}	b_{21}	b_{22}
Prescribed	0.040	0.060	-0.025	0.000
Estimated [Eqs. (9) and (10)]	0.043	0.067	-0.026	-0.002

4. Concluding remarks

The low-frequency variability of the extratropical large-scale circulation is often studied using a reduced-order model of the leading EOF of zonal-mean zonal wind. The key component of this model (LH01) is an internal-to-troposphere eddy–zonal flow interaction mechanism that leads to a positive feedback of EOF1 onto itself, thus increasing the persistence of the annular mode (LH01). However, several studies have shown that under some circumstances, strong couplings exist between EOF1 and EOF2 at some lag times, resulting in decaying-oscillatory, or propagating, annular modes (e.g., Son and Lee 2006; Son et al. 2008; Sheshadri and Plumb 2017). In the current study, following the methodology of LH01 and using data from the SH reanalysis and two setups of an idealized GCM that produce circulations with a dominant nonpropagating or propagating regime, we first show strong cross correlations between EOF1 (EOF2) and the eddy forcing of EOF2 (EOF1) at long lags, suggesting that cross-EOF feedbacks might exist in the propagating regimes. These findings together demonstrate that there is a need to extend the single-EOF model of LH01 and build a model that includes, at a minimum, both leading EOFs and accounts for their cross feedbacks.

With similar assumptions and simplifications used in LH01, we have developed a two-EOF model for propagating annular modes [consisting of a system of two coupled ODEs, Eqs. (4)

TABLE 3. Prescribed feedback strengths (day^{-1}) used to analyze the impact of cross-EOF feedbacks on the decorrelation time scales of z_1 and z_2 . The imposed damping rates of friction are $\tau_1 = \tau_2 = 8$ days.

Feedback	b_{11}	b_{12}	b_{21}	b_{22}
Exp1	0.040	0.000	0.000	0.000
Exp2	0.040	0.060	-0.025	0.000
Exp3	0.040	0.120	-0.050	0.000
Exp4	0.040	0.240	-0.100	0.000
Exp5	0.040	0.480	-0.200	0.000

and (5) with Eqs. (7) and (8)] that can account for the cross-EOF feedbacks. In this model, the strength of the feedback of the k th EOF onto the j th EOF is b_{jk} ($j, k = 1, 2$). Using the analytical solution of this model, we derive conditions for the existence of the propagating regime based on the feedback strengths. It is shown that the propagating regime, which requires a decaying-oscillatory solution of the coupled ODEs, can exist only if the cross-EOF feedbacks have opposite signs ($b_{12}b_{21} < 0$), and if and only if the following criterion is satisfied: $(b_{11} - b_{22})^2 < -4b_{12}b_{21}$. These criteria show that nonzero cross-EOF feedbacks are essential components of the propagating regime dynamics.

Using this model and the idealized GCM and a stochastic prototype, we further show that cross-EOF feedbacks play an important role in controlling the persistence of the propagating annular modes (i.e., the e -folding decorrelation time scale of the zonal index z_i) by setting the frequency of the oscillation ω [Eq. (24)]. Therefore, in this regime, the persistence of the annular mode (EOF1) does not only depend on the feedback of EOF1 onto itself, but also depends on the cross-EOF feedbacks. We find that as a result of the oscillation, the stronger the cross-EOF feedbacks, the less persistent the annular mode.

Applying the coupled-EOF model to the reanalysis data shows the existence of strong cross-EOF feedbacks in the

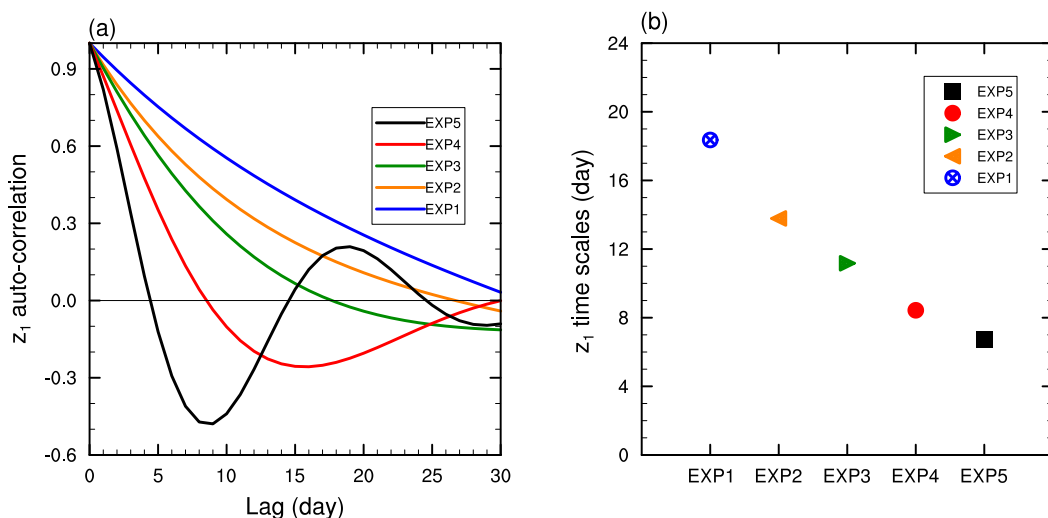


FIG. 11. (a) Autocorrelation functions of z_1 and (b) their corresponding e -folding decorrelation time scales from the analytical solutions [Eqs. (22)–(25)] for the experiment with no cross-EOF feedback (EXP1) and the experiments with increasing cross-EOF feedback strength (EXP2–EXP5). The prescribed feedback strength b_{jk} are shown in Table 3.

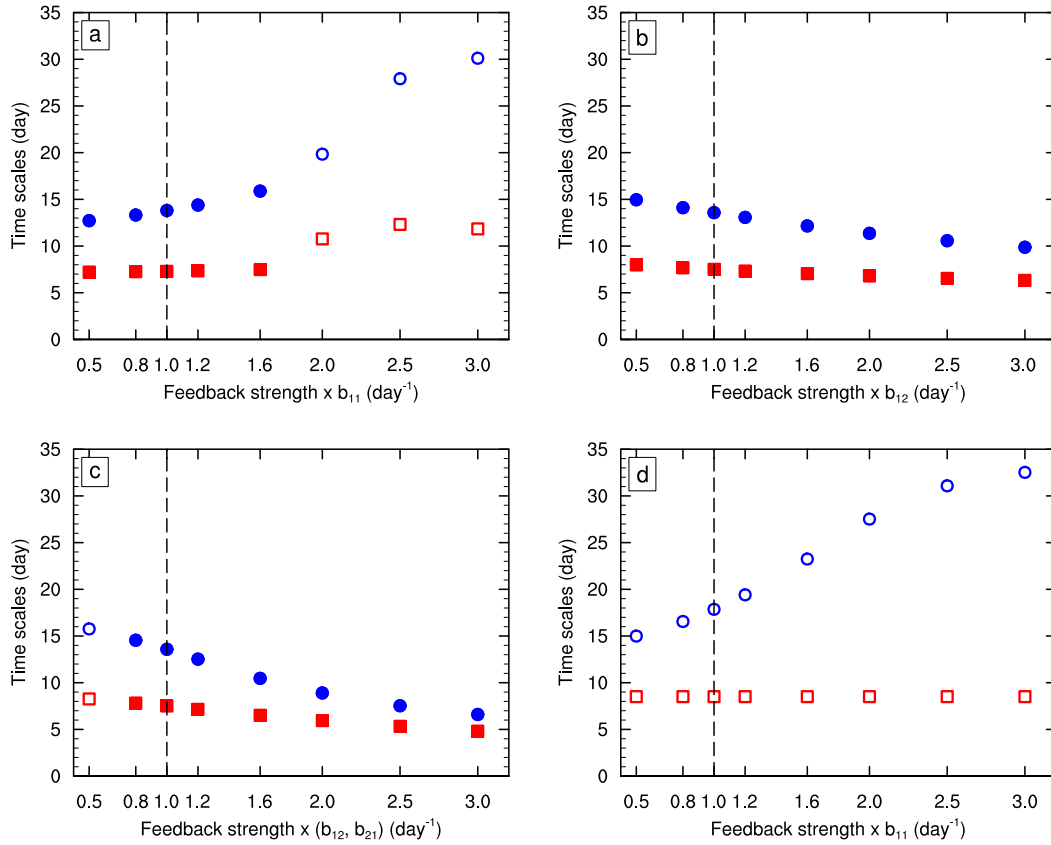


FIG. 12. The computed e -folding decorrelation time scale (days) of z_1 (blue circles) and z_2 (red squares) as a function of feedback strengths (day^{-1}). The impact of varying (a) b_{11} , (b) b_{12} , and (c) b_{12} and b_{21} on the decorrelation time scale (the y axis) while all other b_{jk} are kept the same. The x axis shows the value of varied b_{jk} as fraction of the value in EXP2 (Table 3); the vertical dashed line indicates the control values. (d) The impact of varying b_{11} in EXP1 (Table 3). The filled circles and squares indicate that the parameters satisfy the condition for propagating regimes, i.e., existence of decaying-oscillatory solutions [Eq. (20)].

current SH extratropical large-scale circulation. Annular modes have been found to be too persistent compared to observations in GCMs including IPCC AR4 and CMIP5 models (Gerber and Vallis 2007; Gerber et al. 2008a; Bracegirdle et al. 2020). This long persistence has been often attributed to a too-strong positive EOF1-onto-EOF1 feedback in the GCMs. The dynamics and strength of this feedback depends on factors such as the mean flow and surface friction (Robinson 2000; LH01; Chen and Plumb 2009; Hassanzadeh and Kuang 2019). External (to the troposphere) influence, e.g., from the stratospheric polar vortex, has been also suggested to affect the persistence of the annular modes (Baldwin et al. 2003; Simpson et al. 2011; Byrne et al. 2016; Saggioro and Shepherd 2019).

TABLE 4. Feedback strengths (day^{-1}) estimated for year-round ERA-Interim. The damping rates of friction are estimated as $\tau_1 = 8.3$ days and $\tau_2 = 8.4$ days following the methodology in the appendix of LH01.

Feedback	b_{11}	b_{12}	b_{21}	b_{22}
Eqs. (9) and (10)	0.038	0.059	−0.020	0.017
LH01	0.035	—	—	0.002

Our results show that the cross-EOF feedbacks play an important role in the dynamics of the annular modes, and in particular, that their absence or weak amplitudes can increase the persistence, offering another explanation for the too-persistent annular modes in GCMs.

Overall, our findings demonstrate that to fully understand the dynamics of the large-scale extratropical circulation and the reason(s) behind the too-persistent annular modes in GCMs, the coupling of the leading EOFs and the cross-EOF feedbacks should be examined using models such as the one

TABLE 5. Feedback strengths (day^{-1}) estimated for the idealized GCM setups with nonpropagating and propagating regimes. The estimated damping rates of friction are $\tau_1 = 7.4$ days and $\tau_2 = 7.6$ days for the GCM setup with nonpropagating regime, and $\tau_1 = 7.1$ days and $\tau_2 = 7.4$ days for the GCM setup with propagating regime (estimated using the methodology in the appendix of LH01).

Feedback	b_{11}	b_{12}	b_{21}	b_{22}
Nonpropagating	0.133	0.003	0.002	0.021
Propagating	0.101	0.075	−0.043	0.023

introduced in this study. Note that processes other than internal (to the troposphere) eddy–zonal flow feedbacks [e.g., those suggested by Byrne et al. (2016) and Saggioro and Shepherd (2019)] could be also included in these models as external forcings to build more complete models for the large-scale extratropical variability.

An important next step is to investigate the underlying dynamics of the cross-EOF feedbacks. So far, we have pointed out that cross-EOF feedbacks are essential components of the propagating annular modes; however, the propagation itself is likely essential for the existence of cross-EOF feedbacks. In fact, our preliminary analysis shows that the cross-EOF feedbacks result from the out-of-phase oscillations of EOF1 (north–south jet displacement) and EOF2 (jet pulsation) leading to an orchestrated combination of equatorward propagation of wave activity (a baroclinic process) and nonlinear wave breaking (a barotropic process), which altogether act to reduce the total eddy forcings (not shown). In ongoing work, we aim to explain and quantify the propagating annular modes dynamics using the LRF framework of Hassanzadeh and Kuang (2016b,a) and finite-amplitude wave-activity framework (Nakamura and Zhu 2010; Lubis et al. 2018a,b) that have been proven useful in understanding the dynamics of the nonpropagating annular modes (Nie et al. 2014; Ma et al. 2017; Hassanzadeh and Kuang 2019).

Acknowledgments. We thank Aditi Sheshadri, Ding Ma, and Orli Lachmy for insightful discussions and Ebrahim Nabizadeh for helpful comments on the manuscript. We are grateful to three anonymous reviewers for providing valuable feedbacks and suggestions. This work is supported by National Science Foundation (NSF) Grant AGS-1921413. Computational resources were provided by XSEDE (allocation ATM170020), NCAR's CISL (allocation URIC0004), and Rice University Center for Research Computing.

APPENDIX

Standard Errors of Cross Correlations using Bartlett's Formula

Assuming two stationary normal time series $\{X_t\}$ and $\{Y_t\}$ ($t \in [0, T]$) with the corresponding autocorrelation functions $\rho_X(l)$ and $\rho_Y(l)$ and zero true cross correlations, the standard error of the estimated cross correlation at lag l ($r_{XY}(l)$) can be computed as (see Bartlett 1978, p. 352):

$$\text{var}\{r_{XY}(l)\} = \frac{1}{T - |l|} \sum_{g=-\infty}^{\infty} [\rho_X(g)\rho_Y(g)]. \quad (\text{A1})$$

The null hypothesis is $r_{XY}(l) = 0$, and it is rejected at the 5% significance level if the estimated cross-correlation value at lag l is larger than 2 times the square root of the estimated standard error, i.e., $|r_{XY}(l)| > 2 \times \sqrt{\text{var}\{r_{XY}(l)\}}$.

REFERENCES

- Baldwin, M. P., D. B. Stephenson, D. W. J. Thompson, T. J. Dunkerton, A. J. Charlton, and A. O'Neill, 2003: Stratospheric memory and skill of extended-range weather forecasts. *Science*, **301**, 636–640, <https://doi.org/10.1126/science.1087143>.
- Bartlett, M. S., 1978: *An Introduction to Stochastic Processes with Special Reference to Methods and Applications*. By M. S. Bartlett. *J. Inst. Actuaries*, **81**, 198–199, <https://doi.org/10.1017/S0020268100035964>.
- Boljka, L., T. G. Shepherd, and M. Blackburn, 2018: On the coupling between barotropic and baroclinic modes of extratropical atmospheric variability. *J. Atmos. Sci.*, **75**, 1853–1871, <https://doi.org/10.1175/JAS-D-17-0370.1>.
- Bracegirdle, T. J., C. R. Holmes, J. S. Hosking, G. J. Marshall, M. Osman, M. Patterson, and T. Rackow, 2020: Improvements in circumpolar Southern Hemisphere extratropical atmospheric circulation in CMIP6 compared to CMIP5. *Earth Space Sci.*, **7**, e2019EA001065, <https://doi.org/10.1029/2019EA001065>.
- Branstator, G., 1995: Organization of storm track anomalies by recurring low-frequency circulation anomalies. *J. Atmos. Sci.*, **52**, 207–226, [https://doi.org/10.1175/1520-0469\(1995\)052<0207:OOSTAB>2.0.CO;2](https://doi.org/10.1175/1520-0469(1995)052<0207:OOSTAB>2.0.CO;2).
- Burrows, D. A., G. Chen, and L. Sun, 2016: Barotropic and baroclinic eddy feedbacks in the midlatitude jet variability and responses to climate change–like thermal forcings. *J. Atmos. Sci.*, **74**, 111–132, <https://doi.org/10.1175/JAS-D-16-0047.1>.
- Byrne, N. J., T. G. Shepherd, T. Woollings, and R. A. Plumb, 2016: Annular modes and apparent eddy feedbacks in the Southern Hemisphere. *Geophys. Res. Lett.*, **43**, 3897–3902, <https://doi.org/10.1002/2016GL068851>.
- Chen, G., and R. A. Plumb, 2009: Quantifying the eddy feedback and the persistence of the zonal index in an idealized atmospheric model. *J. Atmos. Sci.*, **66**, 3707–3720, <https://doi.org/10.1175/2009JAS3165.1>.
- Dee, D. P., and Coauthors, 2011: The ERA-Interim reanalysis: Configuration and performance of the data assimilation system. *Quart. J. Roy. Meteor. Soc.*, **137**, 553–597, <https://doi.org/10.1002/qj.828>.
- Feldstein, S. B., 1998: An observational study of the intraseasonal poleward propagation of zonal mean flow anomalies. *J. Atmos. Sci.*, **55**, 2516–2529, [https://doi.org/10.1175/1520-0469\(1998\)055<2516:AOSOTI>2.0.CO;2](https://doi.org/10.1175/1520-0469(1998)055<2516:AOSOTI>2.0.CO;2).
- , and S. Lee, 1998: Is the atmospheric zonal index driven by an eddy feedback? *J. Atmos. Sci.*, **55**, 3077–3086, [https://doi.org/10.1175/1520-0469\(1998\)055<3077:ITAZID>2.0.CO;2](https://doi.org/10.1175/1520-0469(1998)055<3077:ITAZID>2.0.CO;2).
- Gerber, E. P., and G. K. Vallis, 2007: Eddy–zonal flow interactions and the persistence of the zonal index. *J. Atmos. Sci.*, **64**, 3296–3311, <https://doi.org/10.1175/JAS4006.1>.
- , L. M. Polvani, and D. Ancukiewicz, 2008a: Annular mode time scales in the Intergovernmental Panel on Climate Change Fourth Assessment Report models. *Geophys. Res. Lett.*, **35**, L22707, <https://doi.org/10.1029/2008GL035712>.
- , S. Voronin, and L. M. Polvani, 2008b: Testing the annular mode autocorrelation time scale in simple atmospheric general circulation models. *Mon. Wea. Rev.*, **136**, 1523–1536, <https://doi.org/10.1175/2007MWR2211.1>.
- Hassanzadeh, P., and Z. Kuang, 2016a: The linear response function of an idealized atmosphere. Part I: Construction using Green's functions and applications. *J. Atmos. Sci.*, **73**, 3423–3439, <https://doi.org/10.1175/JAS-D-15-0338.1>.
- , and —, 2016b: The linear response function of an idealized atmosphere. Part II: Implications for the practical use of the fluctuation–dissipation theorem and the role of operator's nonnormality. *J. Atmos. Sci.*, **73**, 3441–3452, <https://doi.org/10.1175/JAS-D-16-0099.1>.
- , and —, 2019: Quantifying the annular mode dynamics in an idealized atmosphere. *J. Atmos. Sci.*, **76**, 1107–1124, <https://doi.org/10.1175/JAS-D-18-0268.1>.

- Hasselmann, K., 1988: Pips and pops: The reduction of complex dynamical systems using principal interaction and oscillation patterns. *J. Geophys. Res.*, **93**, 11 015–11 021, <https://doi.org/10.1029/JD093iD09p11015>.
- Held, I. M., 2005: The gap between simulation and understanding in climate modeling. *Bull. Amer. Meteor. Soc.*, **86**, 1609–1614, <https://doi.org/10.1175/BAMS-86-11-1609>.
- , and M. J. Suarez, 1994: A proposal for the intercomparison of the dynamical cores of atmospheric general circulation models. *Bull. Amer. Meteor. Soc.*, **75**, 1825–1830, [https://doi.org/10.1175/1520-0477\(1994\)075<1825:APFTIO>2.0.CO;2](https://doi.org/10.1175/1520-0477(1994)075<1825:APFTIO>2.0.CO;2).
- James, I. N., and J. P. Dodd, 1996: A mechanism for the low-frequency variability of the mid-latitude troposphere. *Quart. J. Roy. Meteor. Soc.*, **122**, 1197–1210, <https://doi.org/10.1002/qj.49712253309>.
- Jeevanjee, N., P. Hassanzadeh, S. Hill, and A. Sheshadri, 2017: A perspective on climate model hierarchies. *J. Adv. Model. Earth Syst.*, **9**, 1760–1771, <https://doi.org/10.1002/2017MS001038>.
- Kidson, J. W., 1988: Interannual variations in the Southern Hemisphere circulation. *J. Climate*, **1**, 1177–1198, [https://doi.org/10.1175/1520-0442\(1988\)001<1177:IVITSH>2.0.CO;2](https://doi.org/10.1175/1520-0442(1988)001<1177:IVITSH>2.0.CO;2).
- Lee, S., S.-W. Son, K. Grise, and S. B. Feldstein, 2007: A mechanism for the poleward propagation of zonal mean flow anomalies. *J. Atmos. Sci.*, **64**, 849–868, <https://doi.org/10.1175/JAS3861.1>.
- Limpasuvan, V., and D. L. Hartmann, 1999: Eddies and the annular modes of climate variability. *Geophys. Res. Lett.*, **26**, 3133–3136, <https://doi.org/10.1029/1999GL010478>.
- Lindgren, E. A., A. Sheshadri, and R. A. Plumb, 2020: Frequency-dependent behavior of zonal jet variability. *Geophys. Res. Lett.*, **47**, e2019GL086585, <https://doi.org/10.1029/2019GL086585>.
- Lorenz, D. J., 2014: Understanding midlatitude jet variability and change using Rossby wave chromatography: Wave–mean flow interaction. *J. Atmos. Sci.*, **71**, 3684–3705, <https://doi.org/10.1175/JAS-D-13-0201.1>.
- , and D. L. Hartmann, 2001: Eddy–zonal flow feedback in the Southern Hemisphere. *J. Atmos. Sci.*, **58**, 3312–3327, [https://doi.org/10.1175/1520-0469\(2001\)058<3312:EZFFIT>2.0.CO;2](https://doi.org/10.1175/1520-0469(2001)058<3312:EZFFIT>2.0.CO;2).
- , and —, 2003: Eddy–zonal flow feedback in the Northern Hemisphere winter. *J. Climate*, **16**, 1212–1227, [https://doi.org/10.1175/1520-0442\(2003\)16<1212:EFFFITN>2.0.CO;2](https://doi.org/10.1175/1520-0442(2003)16<1212:EFFFITN>2.0.CO;2).
- Lubis, S. W., C. S. Y. Huang, N. Nakamura, N.-E. Omrani, and M. Jucker, 2018a: Role of finite-amplitude Rossby waves and nonconservative processes in downward migration of extratropical flow anomalies. *J. Atmos. Sci.*, **75**, 1385–1401, <https://doi.org/10.1175/JAS-D-17-0376.1>.
- , —, and —, 2018b: Role of finite-amplitude eddies and mixing in the life cycle of stratospheric sudden warmings. *J. Atmos. Sci.*, **75**, 3987–4003, <https://doi.org/10.1175/JAS-D-18-0138.1>.
- Ma, D., P. Hassanzadeh, and Z. Kuang, 2017: Quantifying the eddy–jet feedback strength of the annular mode in an idealized GCM and reanalysis data. *J. Atmos. Sci.*, **74**, 393–407, <https://doi.org/10.1175/JAS-D-16-0157.1>.
- Nakamura, N., and D. Zhu, 2010: Finite-amplitude wave activity and diffusive flux of potential vorticity in eddy–mean flow interaction. *J. Atmos. Sci.*, **67**, 2701–2716, <https://doi.org/10.1175/2010JAS3432.1>.
- Nie, Y., Y. Zhang, G. Chen, X.-Q. Yang, and D. A. Burrows, 2014: Quantifying barotropic and baroclinic eddy feedbacks in the persistence of the southern annular mode. *Geophys. Res. Lett.*, **41**, 8636–8644, <https://doi.org/10.1002/2014GL062210>.
- Penland, C., 1989: Random forcing and forecasting using principal oscillation pattern analysis. *Mon. Wea. Rev.*, **117**, 2165–2185, [https://doi.org/10.1175/1520-0493\(1989\)117<2165:RFAPUP>2.0.CO;2](https://doi.org/10.1175/1520-0493(1989)117<2165:RFAPUP>2.0.CO;2).
- Robert, L., G. Rivière, and F. Codron, 2017: Positive and negative eddy feedbacks acting on midlatitude jet variability in a three-level quasigeostrophic model. *J. Atmos. Sci.*, **74**, 1635–1649, <https://doi.org/10.1175/JAS-D-16-0217.1>.
- Robinson, W. A., 1991: The dynamics of the zonal index in a simple model of the atmosphere. *Tellus*, **43A**, 295–305, <https://doi.org/10.3402/tellusa.v43i5.11953>.
- , 2000: A baroclinic mechanism for the eddy feedback on the zonal index. *J. Atmos. Sci.*, **57**, 415–422, [https://doi.org/10.1175/1520-0469\(2000\)057<0415:ABMFTE>2.0.CO;2](https://doi.org/10.1175/1520-0469(2000)057<0415:ABMFTE>2.0.CO;2).
- Ronalds, B., E. Barnes, and P. Hassanzadeh, 2018: A barotropic mechanism for the response of jet stream variability to Arctic amplification and sea ice loss. *J. Climate*, **31**, 7069–7085, <https://doi.org/10.1175/JCLI-D-17-0778.1>.
- Saggioro, E., and T. G. Shepherd, 2019: Quantifying the timescale and strength of Southern Hemisphere intraseasonal stratosphere–troposphere coupling. *Geophys. Res. Lett.*, **46**, 13 479–13 487, <https://doi.org/10.1029/2019GL084763>.
- Sheshadri, A., and R. A. Plumb, 2017: Propagating annular modes: Empirical orthogonal functions, principal oscillation patterns, and time scales. *J. Atmos. Sci.*, **74**, 1345–1361, <https://doi.org/10.1175/JAS-D-16-0291.1>.
- Simpson, I. R., P. Hitchcock, T. G. Shepherd, and J. F. Scinocca, 2011: Stratospheric variability and tropospheric annular-mode timescales. *Geophys. Res. Lett.*, **38**, L20806, <https://doi.org/10.1029/2011GL049304>.
- , T. G. Shepherd, P. Hitchcock, and J. F. Scinocca, 2013: Southern annular mode dynamics in observations and models. Part II: Eddy feedbacks. *J. Climate*, **26**, 5220–5241, <https://doi.org/10.1175/JCLI-D-12-00495.1>.
- Son, S.-W., and S. Lee, 2006: Preferred modes of variability and their relationship with climate change. *J. Climate*, **19**, 2063–2075, <https://doi.org/10.1175/JCLI3705.1>.
- , —, S. B. Feldstein, and J. E. Ten Hoeve, 2008: Time scale and feedback of zonal–mean–flow variability. *J. Atmos. Sci.*, **65**, 935–952, <https://doi.org/10.1175/2007JAS2380.1>.
- Sparrow, S., M. Blackburn, and J. D. Haigh, 2009: Annular variability and eddy–zonal flow interactions in a simplified atmospheric GCM. Part I: Characterization of high- and low-frequency behavior. *J. Atmos. Sci.*, **66**, 3075–3094, <https://doi.org/10.1175/2009JAS2953.1>.
- Thompson, D. W. J., and J. M. Wallace, 1998: The Arctic oscillation signature in the wintertime geopotential height and temperature fields. *Geophys. Res. Lett.*, **25**, 1297–1300, <https://doi.org/10.1029/98GL00950>.
- , and —, 2000: Annular modes in the extratropical circulation. Part I: month-to-month variability. *J. Climate*, **13**, 1000–1016, [https://doi.org/10.1175/1520-0442\(2000\)013<1000:AMITEC>2.0.CO;2](https://doi.org/10.1175/1520-0442(2000)013<1000:AMITEC>2.0.CO;2).
- , and E. A. Barnes, 2014: Periodic variability in the large-scale Southern Hemisphere atmospheric circulation. *Science*, **343**, 641–645, <https://doi.org/10.1126/science.1247660>.
- , and J. D. Woodworth, 2014: Barotropic and baroclinic annular variability in the Southern Hemisphere. *J. Atmos. Sci.*, **71**, 1480–1493, <https://doi.org/10.1175/JAS-D-13-0185.1>.
- , and Y. Li, 2015: Baroclinic and barotropic annular variability in the Northern Hemisphere. *J. Atmos. Sci.*, **72**, 1117–1136, <https://doi.org/10.1175/JAS-D-14-0104.1>.
- Zurita-Gotor, P., 2014: On the sensitivity of zonal-index persistence to friction. *J. Atmos. Sci.*, **71**, 3788–3800, <https://doi.org/10.1175/JAS-D-14-0067.1>.

CORRIGENDUM

SANDRO W. LUBIS^a AND PEDRAM HASSANZADEH^a

^a *Rice University, Houston, Texas*

(Manuscript received 1 March 2023, in final form 1 March 2023)

ABSTRACT: This corrigendum corrects a typo in Eq. (10) of Lubis and Hassanzadeh (2021) for calculating the cross-EOF feedbacks.

We have identified a typographical error in Eq. (10) of Lubis and Hassanzadeh (2021). In the first matrix on the left-hand side of Eq. (10), the two columns should be switched. The correct form of Eq. (10) is

$$\begin{bmatrix} \text{reg}_l(z_1, z_1) & \text{reg}_l(z_2, z_1) \\ \text{reg}_l(z_1, z_2) & \text{reg}_l(z_2, z_2) \end{bmatrix} \begin{bmatrix} b_{21} \\ b_{22} \end{bmatrix} = \begin{bmatrix} \text{reg}_l(m_2, z_1) \\ \text{reg}_l(m_2, z_2) \end{bmatrix}. \quad (1)$$

Nonetheless, all analyses in Lubis and Hassanzadeh (2021) were done using the correct formula; hence, the results are not affected in any way. The authors sincerely apologize for any inconvenience this error may have caused.

REFERENCE

Lubis, S. W., and P. Hassanzadeh, 2021: An eddy–zonal flow feedback model for propagating annular modes. *J. Atmos. Sci.*, **78**, 249–267, <https://doi.org/10.1175/JAS-D-20-0214.1>.

Lubis's current affiliation: Pacific Northwest National Laboratory, Richland, Washington.

Corresponding author: Sandro W. Lubis, sandro.lubis@pnnl.gov; Pedram Hassanzadeh, pedram@rice.edu

DOI: 10.1175/JAS-D-23-0034.1

For information regarding reuse of this content and general copyright information, consult the [AMS Copyright Policy](https://www.ametsoc.org/PUBSReuseLicenses) (www.ametsoc.org/PUBSReuseLicenses).